2016-06-30

Modeling of Acoustic Resonators and Resonator Systems for Use in Passive Noise Control

Matthew Franklin Calton
Brigham Young University

Modeling of Acoustic Resonators and Resonator Systems for Use in Passive Noise Control

Matthew Franklin Calton

A thesis submitted to the faculty of
Brigham Young University
in partial fulfillment of the requirements for the degree of

Master of Science

Scott D. Sommerfeldt, Chair
Timothy W. Leishman
Jonathan D. Blotter

Department of Physics and Astronomy

Brigham Young University

July 2016

ABSTRACT

Modeling of Acoustic Resonators and Resonator Systems
for Use in Passive Noise Control

Matthew Franklin Calton
Department of Physics and Astronomy, BYU
Master of Science

Acoustic resonators, such as the Helmholtz and quarter-wave resonator, can be used to attenuate unwanted noise in an enclosed space. Classical formulations can be used to approximate resonator performance for a given resonator configuration, but may lack sufficient accuracy for some applications. This research aims to improve the analytical characterization of resonators to provide better correlation to experimental results.

Using higher-order approximations and proper end corrections, more accuracy can be obtained in calculating the impedance and resonance frequency of a single resonator, which will then carry over into the overall configuration of the model. The impedance of a system of resonators in parallel is also considered, where the effects of acoustic coupling can be observed.

Resonators with complex, non-ideal geometries are explored for applications where space is limited. The effects of tapers and toroidal curves are considered using impedance translation methods. These theoretical predictions are found to compare favorably with empirical data.

Coupling between an enclosure and resonator system is explored experimentally. The effects of resonator placement, damping, and relative cavity and enclosure volume are considered. These data are used to design and test a resonator system with 10 dB of attenuation over a bandwidth of 10 Hz.

Keywords: resonator, impedance translation, resonator-enclosure coupling, Helmholtz, two-microphone method, lumped element

ACKNOWLEDGMENTS

The author would like to first thank his advisor, Dr. Scott Sommerfeldt, for all the assistance and guidance he has provided over the last few years. He would also like to express gratitude to Dr. Tim Leishman for the advice and expertise imparted over the course of this project. The author would like to thank Dr. Jon Blotter for imparting his knowledge of noise control engineering. The financial support of Caterpillar Inc. was essential in the completion of this thesis.

The contributions of Zac Jensen, Josh Bodon, Kyle Miller, Kelli Succo, Sarah Young, and Steven Markham are greatly appreciated. Finally, the author would like to wholeheartedly thank his wonderful wife for her unwavering love and support.

Contents

List of Figures

List of Tables

Chapter 1

Introduction

1.1 Motivation

In recent years, noise control has become the focus of substantial research. Its effect on human health and comfort has led to the creation and implementation of numerous noise control methods. In general, noise control is achieved by affecting the sources of unwanted sound, impeding sound propagation into sensitive spaces, or transferring sound into other forms of energy. Depending on the nature of the system, one or more noise control strategies may be employed.

Noise control methods have been applied to a wide range of problems. For example, barriers have been constructed along highways to attenuate noise from passing vehicles. Residential buildings often install sound-isolating windows and partitions to decrease noise from the exterior. Manufacturers of items such as vacuums and blenders often employ noise control techniques to diminish the sound radiated from their products.

The current research aims to control tonal noise in vehicle interiors. In such applications, the noise usually shifts over time and under different operating conditions. This study is interested in controlling noise around the 100 Hz range within a band of about 10–15 Hz. The desired

attenuation is approximately 9 dB at the peak, and at least 5 dB of attenuation at either extreme of the frequency range of interest.

Most vehicle interiors have very little available space for large acoustic treatments. Most manufacturers also prefer to avoid potential solutions with complicated moving parts, as this would add the need for technicians and regular maintenance. With these constraints in mind, we examine the two main categories under the topic of noise control: active noise control (ANC) and passive noise control.

Active noise control is achieved by introducing phase-shifted acoustic waves from secondary sources to attenuate unwanted sound. The primary noise source is monitored with sensors, which provide a reference signal to the digital signal processing unit that drives the secondary sources [1]. For example, in order to attenuate noise from the engine, the engine tachometer signal could be used as the reference input. This reference signal would be altered through digital signal processing to provide the control signals for the secondary sources installed in the vehicle interior. Error sensors near the operating position would then be used to adaptively update the control filter.

Active noise control is attractive because it offers low-frequency attenuation using relatively small parts. Currently, these techniques are being successfully implemented to attenuate noise from numerous mechanical devices including computer fans, generators, automobiles, and appliances [2, 3].

Among the disadvantages of active noise control are the practical constraints and the balance of performance and complexity [4]. In addition to these drawbacks, most ANC systems require significant hardware that typically requires regular maintenance. Due to these drawbacks and the constraints of the current noise control application, ANC will not be considered as a solution for this work.

Passive noise control methods rely on the response of materials and geometric shapes to absorb or prevent transmission of sound over a specific frequency range. For example, porous ma-

terials are often used to absorb high-frequency sound due to the thermoviscous losses inherent in the medium [5]. Damping treatments are commonly used in architectural applications for high-frequency attenuation, but are often ineffective or impractical for low frequencies.

Resonant absorbers are characterized by a relatively low input impedance to an adjacent sound field at resonance. Waves that propagate into the resonator are then dissipated as heat. Acoustic resonators typically absorb over a very small bandwidth, but are commonly used in applications where noise is constant and tonal. The relatively low cost, durability, and simplicity make passive resonators attractive for noise control purposes.

Some disadvantages for passive noise control include the size and weight of treatments, narrow effective bandwidths, and fixed frequencies. Since the engine noise is tonal and fairly constant, passive noise control offers a viable solution for the current application. However, traditional absorbers are not viable because of the limited space in vehicle interiors. Therefore, acoustic resonators will be examined and modified to produce a desirable bandwidth while remaining within space constraints.

1.2 Background

1.2.1 History of Acoustic Resonators

Acoustic resonators have been the subject of extensive research for decades. Even before formal research was conducted into their design, the ancient Greeks and Romans used them for amplifying specific frequencies and controlling reverberation in their theaters [6–8].

In 1877, Hermann von Helmholtz—from whom the Helmholtz resonator derives its name—used acoustic resonators to study the harmonic components of vibrating objects and musical instruments [9]. Years later, Lord Rayleigh used Helmholtz resonators to determine the resonance frequencies and mode shapes of bells [10]. He also improved the lumped-element, theoretical

predictions for resonance frequency by deriving an end correction which is widely used to this day.

Beginning in the mid-20th century, acoustic resonators became the subject of modern research. Ingard published several papers detailing the effect of various apertures and geometries on the response of traditional resonators [11, 12]. Alster provided theoretical improvements to the classical calculation of resonance frequency in Helmholtz resonators [13]. Meanwhile, Tang applied rigorous, higher-order approximations to various acoustic resonators in hopes of solving rocket combustion instability [14].

As modern industrial design and competition dictate lower noise tolerances, researchers continue to revisit theoretical models of acoustic resonators [15–18]. These rigorous analytical studies, coupled with new computational methods such as the boundary element method (BEM) and finite element analysis (FEA), have enhanced understanding of resonator acoustic responses [19].

1.2.2 Types of Resonators

The two most commonly studied resonators are the Helmholtz and quarter-wave resonators. Due to their widespread use and importance to this research, a qualitative introduction of these resonators is given here. Several additional acoustic resonators are mentioned to provide further background to the subject.

A Helmholtz resonator consists of a cavity of relatively large volume that is connected to a neck or aperture as seen in Fig. 1.1a. A very simple example of a Helmholtz resonator is a soda bottle. When one blows across the open end, the bottle resonates at a well-defined frequency, commonly known as the resonance frequency. Depending on the configuration, a Helmholtz resonator can be made to absorb sound at resonance.

The traditional model used for predicting the response of a Helmholtz resonator is a damped mass-spring oscillator. In this model, the plug of air in the neck acts as a mass while the volume

of air in the cavity acts as the spring. Damping arises from thermoviscous losses at the tube walls, primarily from the motion of the plug of air in the neck.

Similar to a damped mass-spring oscillator, the maximum response of a typical Helmholtz resonator occurs over a relatively small bandwidth. Small errors in the approximation of resonance frequency could cause a target frequency to lie outside of the Helmholtz resonator's attenuating bandwidth. Therefore, special consideration must be taken while designing a Helmholtz resonator for a specific application.

The response of a Helmholtz resonator may be broadened by introducing additional damping. This usually takes the form of some flow-resistive material placed in or near the neck opening. As with a damped mass-spring oscillator, increasing damping in the resonator tends to broaden the working bandwidth while decreasing overall efficiency at resonance [20]. Multiple Helmholtz resonators with closely tuned resonance frequencies have also been employed to increase the working bandwidth [21–23].

A quarter-wave resonator is a simple tube that is open at one end and closed at the other as seen in Fig. 1.1b. Most typical quarter-wave resonators have a relatively constant cross-sectional area over their lengths. Reflections from the boundaries at each end result in standing waves at certain resonance frequencies. These resonances occur when the tube length corresponds to one-fourth of a wavelength. Resonances also occur for every additional half wavelength beyond the fundamental [24]. Again, thermoviscous losses at the tube walls are the primary mechanism for attenuation.

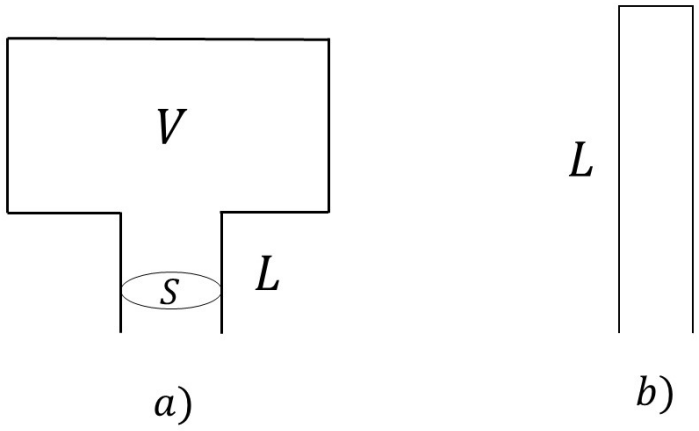

Figure 1.1 A simple representation of (a) a Helmholtz resonator and (b) a quarter-wave tube.

Although the aforementioned resonators are the most common, other resonators have been used and studied in various applications. For example, the Herschel-Quincke tube—depicted in Fig. 1.2—is a parallel connection of two pipes of different lengths and cross-sectional areas [25]. When the difference in path length equals a half wavelength, destructive interference occurs downstream [26].

Another example of an acoustic resonator is the panel absorber. Panel absorbers are typically made of hard, flat materials with many small perforations as seen in Fig. 1.3. The small mass of air in each perforation oscillates in the panel to provide absorption. These panels can have relatively large absorbing bandwidths compared to other traditional acoustic resonators [27].

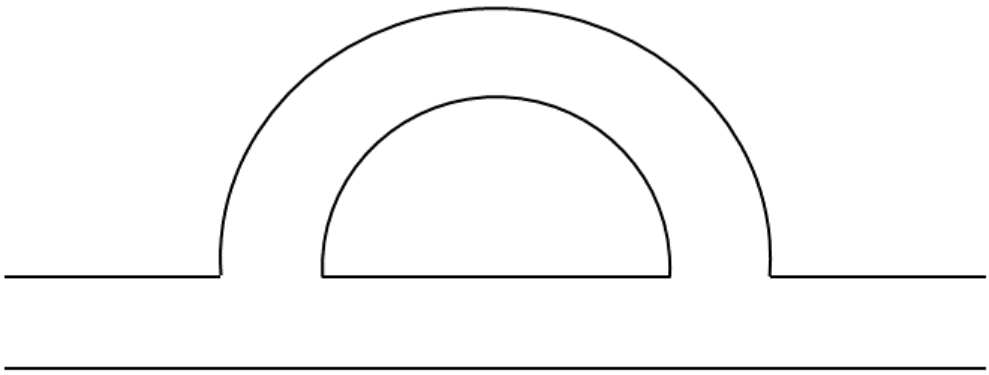

Figure 1.2 A simple representation of a Herschel-Quincke tube.

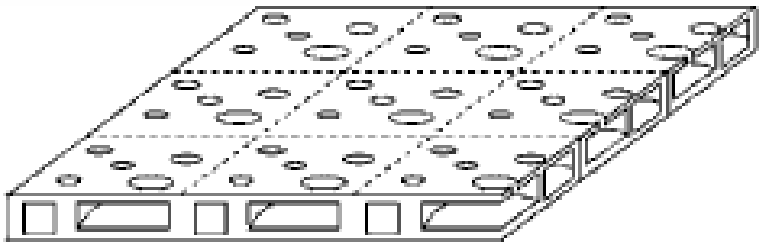

Figure 1.3 Cross section of a typical panel absorber [22].

1.2.3 Uses of Resonators

Acoustic resonators have been implemented in a wide range of noise control applications. Due to their limited bandwidths, engineers have often used them to attenuate stationary noise with strong tonal components. Acoustic resonators are also employed as noise control elements in harsh environments, where sensitive active noise control elements may become damaged.

One application for acoustic resonators is in controlling HVAC duct noise. Dissipative elements such as duct liners or silencers absorb effectively at high frequencies, but are inadequate for low-frequency noise. While some hybrid reactive silencers are being developed [28, 29], such systems have not yet been widely implemented.

When implemented in a side-branch configuration, Helmholtz and quarter-wave resonators may attenuate low-frequency machine noise. Parallel and series arrays of Helmholtz resonators have also been shown to reduce noise in a relatively large band when each resonator is tuned to a slightly different frequency [21]. However, due to their size and sensitivity to tuning, Helmholtz resonators have not seen widespread use in HVAC applications.

A more common use of acoustic resonators in HVAC systems is the expansion chamber seen in Fig. 1.4. These elements consist of a rapid change in cross-sectional area to minimize transmission downstream. Expansion chambers have been shown to provide effective attenuation at low frequencies with a relatively large effective bandwidth [30, 31]. Furthermore, expansion chambers are installed inline with existing duct systems and often require less space than Helmholtz resonators.

The automotive industry has benefited greatly from the use of acoustic resonators. Mufflers often operate on the same principle as HVAC expansion chambers. By adjusting the expansion ratio and chamber length, mufflers can achieve considerable attenuation without introducing significant back pressure. Although science and the range of applications has expanded since the first comprehensive study in the mid-20th century [32], research is still being conducted into optimizing

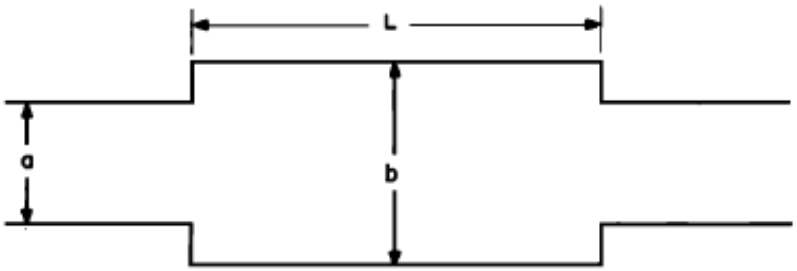

Figure 1.4 A simple representation of an expansion chamber typically found in HVAC systems [30].

space, bandwidth and cost [33].

Acoustic resonators have also been implemented in the attenuation of undesired modes in rooms. These Helmholtz resonators — often referred to as bass-traps — are coupled to spaces to absorb low-frequency sound that would undesirably color sound [34, 35]. Bass-traps are most common in small rooms such as recording studios and listening rooms, although they have also been applied to large concert halls [36].

1.3 Previous Work

Due to their widespread use in engineering and physics, analytical expressions with varying degrees of accuracy have been obtained to predict performance of acoustic resonators. The classical expressions for acoustic resonators derived by Ingard [11, 12] are valid where the dimensions of the resonator are small compared to an acoustic wavelength. However, many researchers have explored the regions wherein resonator geometry and frequency begin to invalidate the classical assumptions.

Karal [37] introduced a frequency-dependent end correction for abrupt changes in cross-sectional area in circular tubes. In 1973, Tang [14] gave a generalized model of the Helmholtz resonator. He compared the theoretical responses of traditional Helmholtz resonators, extended neck

and cavity resonators, and quarter-wave tubes.

Later, Selamet [15] published an in-depth study of three analytical models for different cavity length-to-diameter ratios. He showed that classical end corrections did not account for nonplanar wave propagation at discontinuities. Dickey [38] explored the limit for very small cavity length-to-diameter ratios and provided recommendations for modeling this "pancake" configuration. Meanwhile, Doria [39] provided insights into the analysis of Helmholtz resonators with deep cavities and long necks. Researchers have also studied the cases wherein a resonator neck extends into the cavity [31] and the effects of compartmented, coupled resonators [40].

Furthermore, space constraints in practical applications of acoustic resonators have pushed researchers to obtain new analytical and empirical models for nonideal geometries. Chanaud [41] built on the work of Ingard [11, 12] and Rayleigh [10] to develop resonance equations for atypical orifice and cavity shape. He also provided a table showing expected deviation from traditional expressions given changes to the orifice and cavity geometries. Later, he expanded on this work [42] to develop an expression for the end correction of a cylindrical cavity with an arbitrarily placed orifice. Similar research was conducted recently by Selamet [43], who studied the effect of asymmetric neck placement on Helmholtz resonators. Tang [44] explored the shift in resonance frequency for Helmholtz resonators with tapered necks.

Although very few papers have been written about Helmholtz resonators with curved necks, sound propagation in curved waveguides has been explored extensively. Rostafinski [45] published an article regarding the long wavelength limit demonstrated by Rayleigh. This paper provided the theoretical basis for an infinite bend approximating a coil and a 90° bend followed by an infinite straight duct. Cummings [46] examined curved bends of rectangular and circular cross sections and provided an engineering guide from theory and experiment.

Over the subsequent decade, other studies on curved waveguides were conducted by Osborne [47], Tam [48], Fuller [49], and Cabelli [50]. These studies focused primarily on sound

transmission through curved ducts for use in HVAC systems and other industrial applications. In 1991, Rostafinski compiled much of the previous work into one monograph [51]. In it, he summarizes work done by many researchers to characterize the propagation of sound in curved ducts. The comprehensive article includes analytical and experimental results for angular wavenumber, phase velocity, particle velocity and pressure distributions, and impedance.

Finally, research has been conducted into the coupling between an enclosure and resonator for effective modal attenuation. One of the first theoretical treatments of the topic was provided by Fahy in 1980 [52]. Fahy determined that the most important factors in the coupled problem were related to the ratio of enclosure volume to resonator volume, the modal pressure amplitude at the resonator position, and the damping present in the resonator and enclosure.

Cummings [53] expanded on the work of Fahy with a multi-modal theoretical analysis due to an array of resonators. This analysis was compared to experimental data from past studies and showed favorable agreement. Driesch [54] used optimization techniques to determine the placement and design of Helmholtz resonators in a small enclosure.

Recently, Li [55] developed a model for predicting the response of an enclosure and array of Helmholtz resonators. The solutions for sound pressure in the enclosure and the volume velocity out of the Helmholtz resonator's neck were derived analytically. Data from previous work was used to validate the model. Yu [20] expanded on this model to show the importance of internal damping in the Helmholtz resonator being coupled.

1.4 Overview of Thesis

This thesis aims to provide accurate, computationally efficient methods for modeling systems of acoustic resonators. The techniques presented will improve upon the prediction capabilities for resonators with ideal and nonideal geometries. The methods developed in this research show

considerable improvement in predicting the acoustic impedance of arbitrary systems of resonators when compared to existing approximations. The improved model is then implemented to design a system of resonators for tonal noise control within an enclosure.

1.5 Thesis Organization

Chapter 2 begins with general considerations for modeling sound propagation within acoustic resonators. Various end corrections and loss mechanisms are discussed. It also gives a theoretical basis and experimental validation for acoustic resonators with added damping.

Next, a comparison of methods for modeling ideal-geometry resonators is presented in Chapter 3. The standard lumped-element model is compared to higher-order approximations and impedance translation methods. Elements for combining multiple resonators such as T-junctions are also analyzed. These theoretical models are compared to experimental data. Chapter 4 contains modeling techniques for resonators with nonideal geometries. Helmholtz resonators with tapered and curved necks are modeled and compared with experimental measurements.

Chapter 5 contains a theoretical treatment of the coupled resonator-enclosure system. Primary coupling mechanisms are explained and used to inform the design of practical resonators. The coupled response of the enclosure due to various resonator systems is compared experimentally to the uncoupled case. Finally, conclusions and recommendations are given in Chapter 6.

Chapter 2

General Considerations for Modeling Acoustic Resonators

2.1 End Corrections

Classical theory for a Helmholtz resonator assumes that all acoustic mass is concentrated within the neck. However, the fluid moving within the resonator is not strictly defined by the physical extent of the neck. Therefore, various end corrections have been developed to correct for the added acoustic mass that is expected on each side of the neck.

2.1.1 Classical End Corrections

The classical end correction was originally derived from the radiation impedance seen by an oscillating circular piston. The assumption that the air at the end of the neck behaves similar to a circular piston is valid when the wavelength is large relative to the radius of the pipe [56].

The effective length associated with the additional impedance for the opening of a tube in an

infinite baffle is

$$L_{eff} = L + \frac{8a}{3\pi} \approx L + 0.85a, \tag{2.1}$$

where a is the radius and L is the physical length of the tube. For an unbaffled tube, the typical end correction is given by

$$L_{eff} \approx L + 0.6a. \tag{2.2}$$

These expressions show reasonable agreement for the long-wavelength approximation. Although resonator dimensions may satisfy this approximation, practical implementations often fall between the infinitely baffled and unbaffled cases.

2.1.2 Empirical End Corrections

Empirical end corrections have been developed to address cases where the neck cannot be characterized as infinitely baffled or unbaffled. One simple example of this case is the transition from neck to cavity. For a cylindrical Helmholtz resonator with concentric circular neck and cavity radii, the end correction is given as

$$l_0 = 0.82a(1 - 1.33\xi), \tag{2.3}$$

where ξ is the ratio of the neck diameter to cavity diameter and where $\xi < 0.4$ [43, 57].

For cases where a tube is attached as a side branch to a main duct, analytical expressions are very difficult to obtain. Ji [19] used BEM and experimental data to provide the following expressions:

$$l_0 = a \begin{cases} 0.8216 - 0.0644\xi - 0.694\xi^2; & \xi \leq 0.4 \\ 0.9326 - 0.6196\xi; & \xi > 0.4 \end{cases}, \tag{2.4}$$

where here ξ is the ratio of neck diameter to main duct diameter.

2.1.3 Junction Impedance

Karal [37] derived an analytical expression for the impedance introduced by an abrupt change in circular cross section. Consistent with the previous classical and empirical end corrections, he showed that a mass-like impedance was introduced in series with the tube of smaller radius. The so-called junction impedance is as follows:

$$Z_{AJ} = j\omega M_{AJ}, \tag{2.5}$$

$$M_{AJ} = \frac{8\rho_0}{3\pi^2 a_1} H\left(\frac{a_1}{a_2}\right), \tag{2.6}$$

$$H\left(\frac{a_1}{a_2}\right) = \frac{3\pi}{2} \sum_{m=1}^{\infty} \frac{J_1^2\left(\gamma_m \frac{a_1}{a_2}\right)}{\gamma_m \frac{a_1}{a_2} [\gamma_m J_0(\gamma_m)]^2}, \tag{2.7}$$

where a_1 and a_2 are the radii of the adjoining pipes and γ_m is the m^{th} root of the first-order Bessel function of the first kind. The sum in Eq. (2.7) must be truncated in numerical calculations. In the present research, the sum was truncated when the previous term was smaller than 10^{-10}.

While the classical end corrections are valid for infinitely baffled and unbaffled transitions, Karal's derivation provides detailed predictions over all possible adjoining pipe radii. This provides an accurate characterization of the added acoustic mass over any abrupt change in cross-sectional area.

2.2 Losses in Tubes

In order to create an accurate representation of the predicted response, inherent losses in a resonator system must be considered. There are two primary mechanisms that contribute to losses in a resonator system with plane wave propagation: viscous and thermal damping. Atmospheric absorption due to heat conduction, viscosity, and molecular relaxation has been treated extensively, and analytical and empirical formulations can be found in the literature [58]. For the frequency

range in this study, atmospheric absorption was found to be negligible and is not included in the modeling.

The fluid immediately adjacent to the tube wall is constrained to have zero velocity, a characteristic typically referred to as a no-slip condition. Since each successive fluid element must share the velocity of those with which it is in contact, a viscous boundary layer is created near the wall. In this region, the particle velocity transitions from zero at the tube wall until it matches the particle velocity of the propagating wave. The thickness of this region is often called the acoustic boundary layer thickness or skin depth. It can be calculated from the following equation:

$$\delta_\eta = \sqrt{\frac{2\eta}{\rho_0 \omega}}, \tag{2.8}$$

where η is the coefficient of shear viscosity of air.

Thermal losses occur due to the isothermal behavior of gas near the tube wall. If the wall remains at constant temperature, it acts as an infinite source or sink. Thus, the air immediately adjacent to the wall is also held at constant temperature, creating a small region with a temperature gradient. This differs away from the wall, where waves are adiabatic in nature. Any temperature change due to propagating acoustic waves creates a flow of heat into or out of this thermal region. The thickness of this thermal boundary layer is given by

$$\delta_\kappa = \sqrt{\frac{2\kappa}{\rho_0 \omega c_p}}, \tag{2.9}$$

where κ is the thermal conductivity and c_p is the specific heat for constant pressure of air.

By including the effects of both boundary layers, one can compute the absorption coefficient due to thermal and viscous losses at the tube wall:

$$\alpha_w = \frac{1}{ac}\left(\frac{\eta\omega}{2\rho_0}\right)^{1/2}\left(1+\frac{\gamma-1}{\sqrt{\mathrm{Pr}}}\right), \tag{2.10}$$

where a is the radius of the tube, c is the speed of sound, γ is the ratio of specific heat, and Pr is the Prandtl number given by $\sqrt{\mathrm{Pr}} = \delta_\eta/\delta_\kappa$.

According to Kinsler *et al.* [59], absorptive processes in tubes can be accounted for by replacing the traditional wavenumber k by a complex wavenumber $\tilde{k}$. While there are many formulations for $\tilde{k}$, Kinsler *et al.* simply defined the complex wavenumber as

$$\tilde{k} = \frac{\omega}{c} - j\alpha_w, \tag{2.11}$$

noting that the expression is accurate when $a/\delta_\eta > 10/\sqrt{2}$. This condition holds for the frequencies and resonator dimensions of the present study.

Additional acoustic resistance is introduced due to viscous losses at discontinuities. In the case of a Helmholtz resonator, these losses occur at the junction between the neck and cavity. Depending on the mounting configuration, they may occur at the mouth of the resonator as well. Morse and Ingard [60] derived theoretical expressions for discontinuity losses due to an orifice in thin plates. Bies and Hansen [57] attempted to generalize their results for the discontinuity losses present at the entrance to a tube:

$$R_{A_\eta} = 0.288k\delta_\eta \frac{\rho c}{S_n} \log_{10}\left(\frac{4S_n}{\pi h^2}\right), \tag{2.12}$$

where S_n is the cross-sectional area of the neck and h is either the viscous boundary layer thickness or the neck radius, whichever is larger.

Further acoustic resistance arises due to radiation losses at the mouth of a resonator. Kinsler *et al.* [56] derived the radiation resistance in terms of an infinitely baffled or unbaffled circular piston. These results can be summarized into the following form:

$$R_{A_R} = \varepsilon \frac{S_n k^2}{2\pi}, \tag{2.13}$$

where ε is equal to 1 for the infinitely baffled case and ½ for the unbaffled case. For the purposes of this research, the radiation resistance was considered to be closest to the baffled case. This approximation is valid for resonators coupled to an enclosure where wall dimensions are much larger than an acoustic wavelength. However, the baffled radiation resistance was also applied

to the neck-cavity junction due to magnitude discrepancies observed in measured and theoretical results.

Exact expressions for discontinuity losses and radiation resistance are not available in current literature. Since no analytical expressions or computationally efficient approximations exist for the radiation resistance of a resonator set in a finite baffle, many researchers have used *ad hoc* damping terms [12, 20, 55]. Furthermore, the validity of Bies and Hansen's generalization for discontinuity losses has not been examined. While the acoustic resistance in Eqs. (2.12)–(2.13) show accurate results for the resonators tested in this research, further work should be performed to obtain analytical expressions for each source of acoustic resistance.

2.3 Added Damping

In the design of acoustic resonators and resonator systems, a resistive lining may be added to control the absorbing bandwidth and coupling characteristics of the system. In some cases, various linings can be employed to conceal the opening to an acoustic resonator. Therefore, it is important to accurately predict the effect of added resistance on the overall response of the system.

If the resistive element is placed in contact with the aperture, the aperture resistance will be approximately equal to the airflow resistance, R, of the element [61]. This approximation is valid for materials with low airflow resistance, where the response is purely resistive [62]. As airflow resistance increases, a pressure gradient on either side of the material induces motion. This adds a reactive component to the response of the resistive element. The total response of materials with high airflow resistance may be predicted using both its airflow resistance and mass per unit surface area [63].

Airflow resistance is given in mks acoustic ohms and is the quotient of the air pressure difference across a specimen divided by the volume velocity of airflow through the specimen [64].

Airflow resistivity, r_0, is given in mks rayls/m. It is the product of the airflow resistance of a specimen and its area, divided by its thickness.

The airflow resistance may be obtained from the airflow resistivity data by $R = r_o l/S$, where l is the thickness and S is the cross-sectional area of the sample. This airflow resistance can then be added to the impedance of a Helmholtz resonator to obtain the damped response. Data were measured using ASTM C522.

Several materials were installed in the opening of a simple Helmholtz resonator to validate the formulation above. The neck of the Helmholtz resonator was 15.2 cm in length with a 2 cm radius. The cavity was 17.8 cm in length with a 4.8 cm radius. Results for materials similar to those installed as vehicle interior facings are shown in Figs. 2.1–2.4. The polyester carpet facing and polyethylene terephthalate (PET) substrate are common finish treatments on the interior of many vehicles. PET microfiber facing with PET felt substrate are materials found in similar enclosures. The two-microphone method—described in more detail in Section 3.5—was used to measure input impedance.

The theoretical predictions compare favorably to the measured results. Agreement is readily seen in materials with relatively low airflow resistance. Materials with more airflow resistance tend to shift the resonance peak to lower frequencies. This illustrates that dense materials are also responding as inertances—as opposed to solely resistive elements—adding damping and mass to the original system.

The results shown in Figs. 2.1–2.4 indicate that facing treatments must be carefully selected. While each facing may provide some benefit to the absorbing bandwidth, both substrate materials render the resonator system ineffective. Thus, only materials with low airflow resistance are modeled and applied to the current resonator systems.

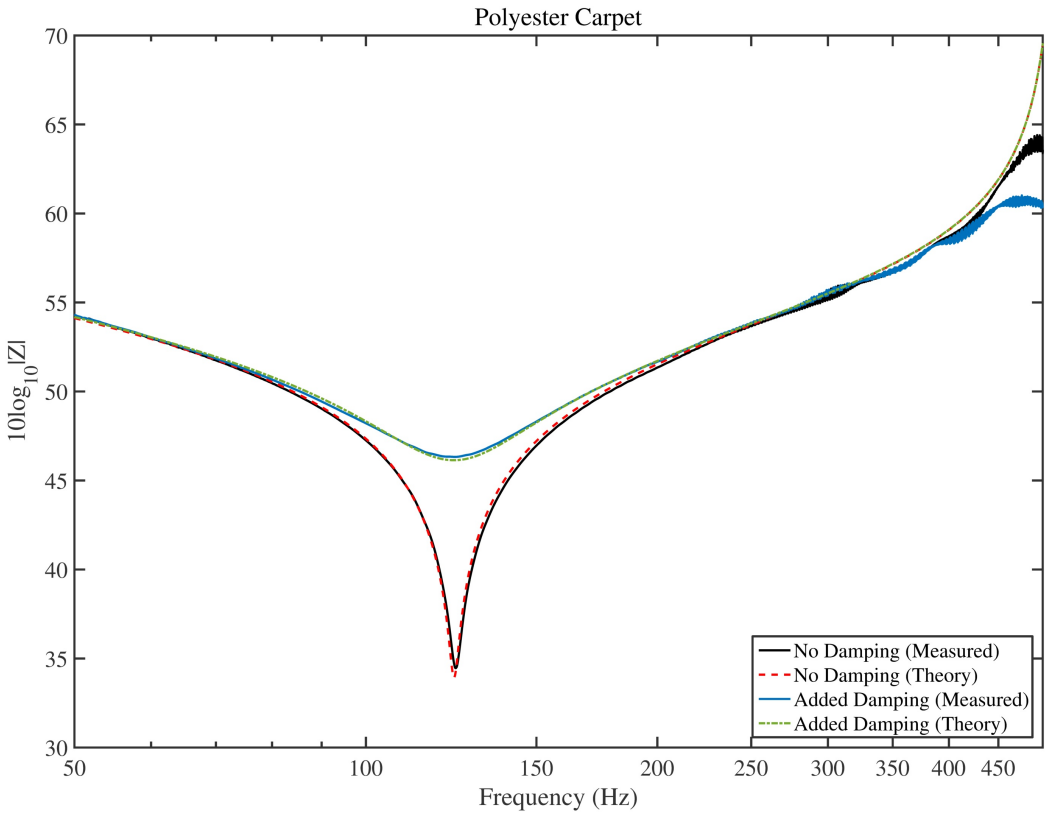

Figure 2.1 Theoretical and measured acoustic impedance for polyester carpet added at the mouth of a single Helmholtz resonator.

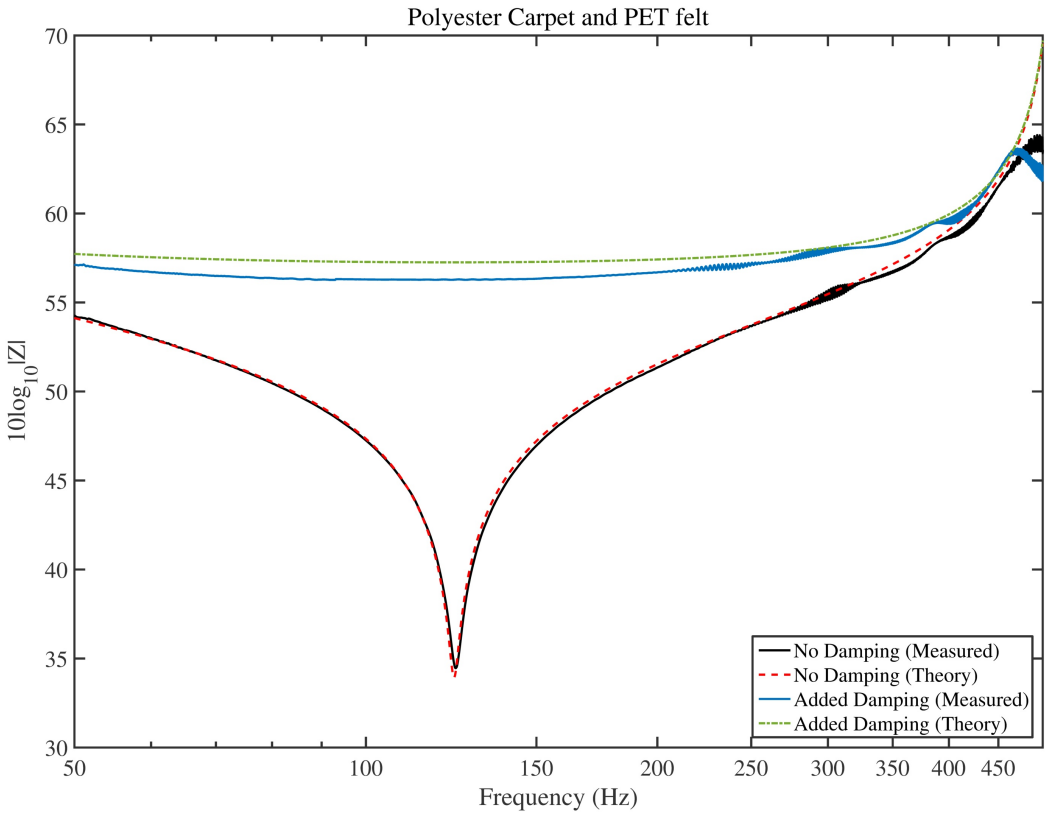

Figure 2.2 Theoretical and measured acoustic impedance for polyester carpet facing and PET felt substrate added at the mouth of a single Helmholtz resonator.

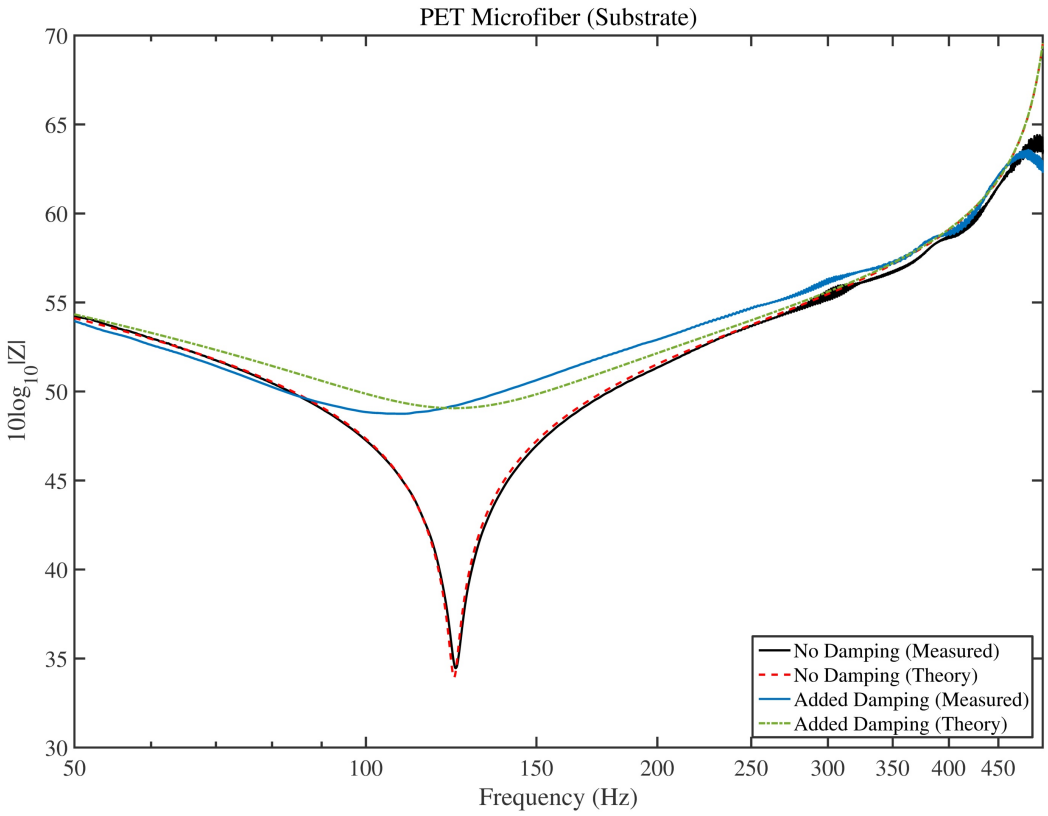

Figure 2.3 Theoretical and measured acoustic impedance for PET microfiber added at the mouth of a single Helmholtz resonator.

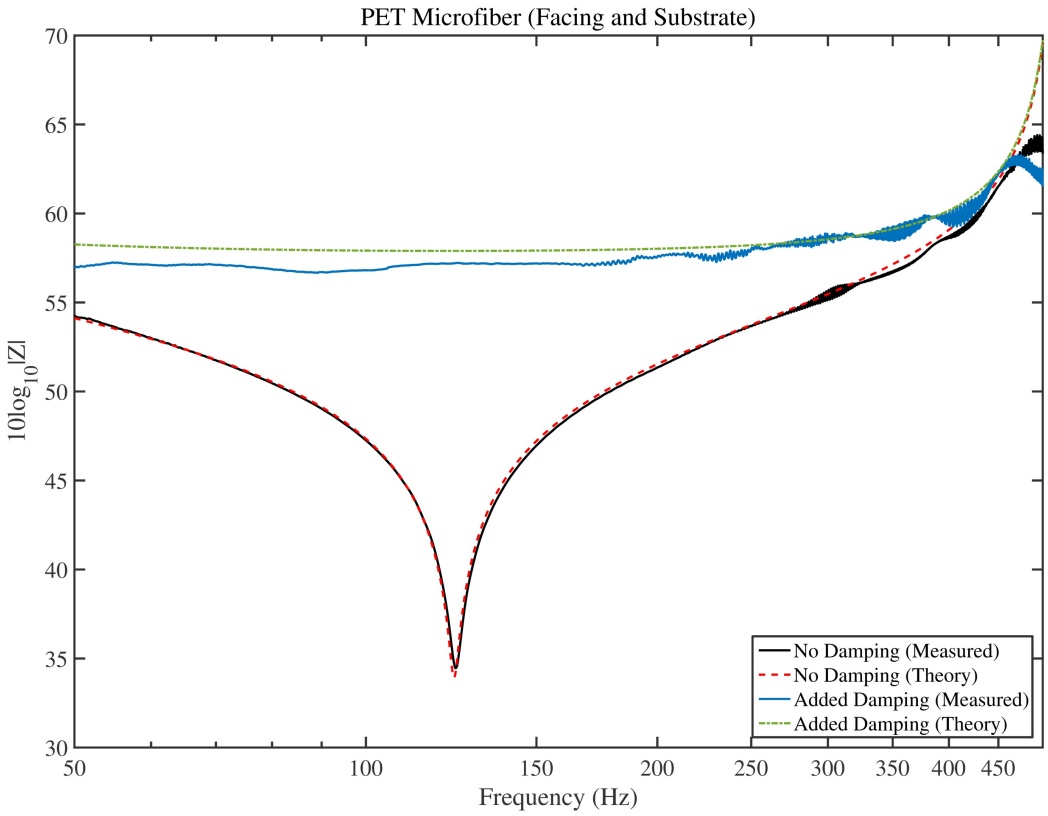

Figure 2.4 Theoretical and measured acoustic impedance for PET microfiber facing and PET felt substrate added at the mouth of a single Helmholtz resonator.

Chapter 3

Modeling of Resonators with Ideal Geometries

In modeling acoustic resonators, their response is often predicted by simple, low-frequency approximations that can yield significant error [13]. Conversely, complicated expressions may add accuracy and detail, albeit at the cost of time and resources. This chapter presents various methods for determining the response of ideal geometry acoustic resonators and systems of resonators. Suggestions are given for choosing between methods. Furthermore, general considerations for accurate resonator system modeling are considered such as end corrections, internal resistance, and added damping.

3.1 Impedance Translation Method

One of the most detailed methods for determining the response of acoustic resonators presented here utilizes impedance translation and waveguide circuits. The impedance translation theorem allows a known impedance to be translated over a length of constant cross-sectional area in order to obtain the impedance at another point in space. The impedance translation theorem is given

mathematically as follows:

$$Z_{A0} = \frac{\rho_0 c}{S} \frac{\frac{Z_{AL}}{\rho_0 c/S} + j \tan \tilde{k} L}{1 + j \frac{Z_{AL}}{\rho_0 c/S} \tan \tilde{k} L}, \tag{3.1}$$

where ρ_0 is the density of air, c is the sound speed, S is the cross-sectional area of the element being considered, L is the length of translation, Z_{AL} is the acoustic impedance before the translation, and Z_{A0} is the input acoustic impedance looking into the system. When $\tilde{k}$ is defined as in Eq. (2.11), thermoviscous losses can be incorporated in the impedance translation.

In the case of an acoustic resonator or system of resonators, many successive translations will occur over different lengths and cross-sectional areas. Therefore, it is convenient to use a circuit representation of the impedance translation theorem. Acoustic pressure is analogous to voltage while volume velocity is analogous to current. Figure 3.1 shows the T-network—referred to as a waveguide circuit—that accomplishes this [65, 66].

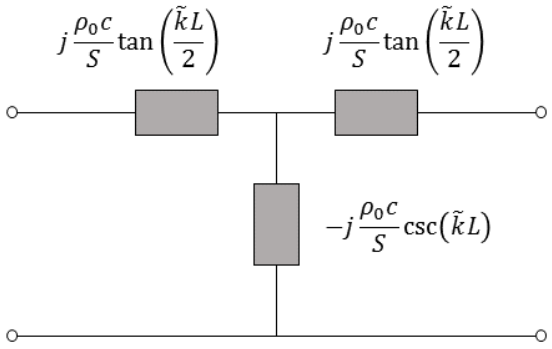

Figure 3.1 T-network or waveguide circuit representation of the impedance translation theorem.

For acoustic resonators such as the Helmholtz resonator, each element can be modeled as a waveguide circuit with the appropriate length and cross-sectional area. After the T-networks have been arranged to reflect the nature of the physical system, parameters such as acoustic impedance can be found at any point in the circuit. Since the waveguide circuit is based on the impedance

translation theorem, all wave effects are preserved throughout the calculations. These formulations and circuits assume that wavelength is large compared to the cross-sectional dimensions of the resonator.

Figure 3.2 shows the entire circuit representation of a simple Helmholtz resonator. The right-most portion of the circuit represents the resonator cavity. The infinite acoustic impedance at the end of the cavity is denoted by an open circuit in the electrical impedance domain. Hence, the final element is discarded because no current will flow through that branch.

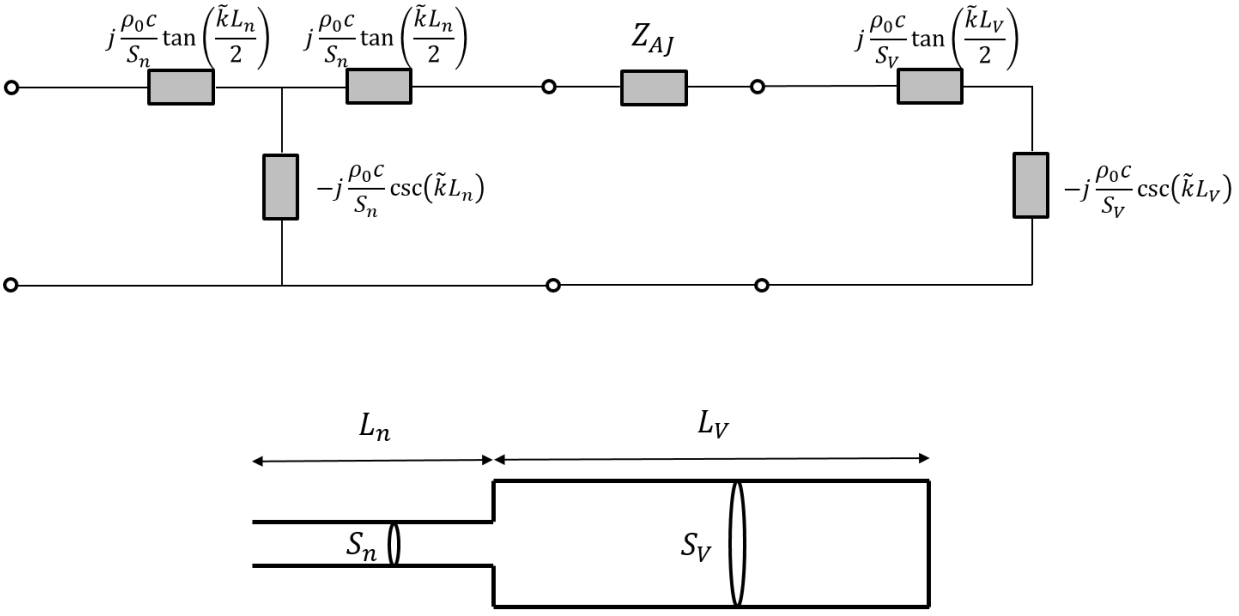

Figure 3.2 Equivalent circuit representation of Helmholtz resonator.

The next circuit element shows the junction impedance of the expansion. The formulation given in Eqs. (2.5)–(2.7) is inserted between the T-networks to account for the additional impedance due to the sudden change in cross-sectional area.

The left-most portion of the circuit represents the impedance translation over the length and cross-sectional area of the neck. In this manner, the acoustic impedance of the entire system, from the end of the cavity to the mouth of the resonator, is modeled as an equivalent circuit.

3.2 Element-by-Element Method

One simplification that can be made to the previous method is to consider the impedance of individual elements in isolation. Instead of translating the impedance over an entire system, one component of the resonator can be viewed separately and added in series or parallel with another component.

As discussed previously, the cavity of a resonator can be considered to have an infinite impedance at one end. Using Eq. (3.1) with an infinite termination impedance, the equation collapses to

$$Z_{A0_{cavity}} = \frac{-j\rho_0 c}{S_V} \cot \tilde{k} L_V, \tag{3.2}$$

for a cavity of length L_V and cross-sectional area S_V.

If the neck of a resonator is viewed in isolation, the impedance at the termination is zero and Eq. (3.1) collapses to:

$$Z_{A0_{neck}} = \frac{j\rho_0 c}{S_n} \tan \tilde{k} L_n, \tag{3.3}$$

for a neck of length L_n and cross-sectional area S_n.

A simple Helmholtz resonator can be modeled using an element-by-element model by adding the acoustic impedance of the neck in series with the acoustic impedance of the cavity. An end correction from the previous chapter should be added for greater accuracy. Therefore, the predicted acoustic impedance of the Helmholtz resonator would be as follows:

$$Z_{AH} = j\rho_0 c \Big(\frac{\tan \tilde{k} L_{n,eff}}{S_n} - \frac{\cot \tilde{k} L_V}{S_V} \Big), \tag{3.4}$$

where $L_{n,eff}$ indicates the inclusion of an end correction.

One limitation of this method is that wave effects are not preserved from element to element. In large systems of resonators, higher-order effects that arise from coupling between two resonators may not be accounted for. In other words, resonances that span multiple acoustic elements will not be accurately modeled.

3.3 Lumped Element Method

The previous method can be simplified even further by assuming that only wavelengths much larger than the dimensions of the pipe will propagate in the system (i.e., $kL \ll 1$). With this assumption, Eqs. (3.2) and (3.3) can be approximated using the first term in their respective Taylor series expansions as follows:

$$Z_{A0_{cavity}} \approx -\frac{j\rho_0 c}{S_V}\frac{1}{kL_V} = \frac{1}{j\omega V/\rho_0 c^2} \tag{3.5}$$

and

$$Z_{A0_{neck}} \approx \frac{j\rho_0 c}{S_n} kL_n = j\omega\frac{\rho_0 L_n}{S_n}, \tag{3.6}$$

where V is the volume of the cavity.

The approximations in Eqs. 3.5 and 3.6 are often used to simplify the acoustic impedance of a Helmholtz resonator into one succinct expression:

$$Z_{AH} = j(\omega M_A - \frac{1}{\omega C_A}) \tag{3.7}$$

with

$$\begin{aligned} M_A &= \frac{\rho_0 L_n}{S_n} \\ C_A &= \frac{V}{\rho_0 c^2}. \end{aligned} \tag{3.8}$$

The plug of air in the resonator neck is represented by the acoustic inertance, M_A, and the enclosed volume of the cavity by the acoustic compliance, C_A. In most applications of the lumped element method, one of the simple end corrections from Eq. (2.1) or Eq. (2.2) is used. Resonance occurs when the reactance of the resonator becomes zero. By setting Eq. (3.7) equal to zero, it is possible to obtain the standard expression for resonance frequency:

$$f_0 = \frac{c}{2\pi}\sqrt{\frac{S_n}{L_{n,eff}V}}. \tag{3.9}$$

When the dimensions of the resonator are not small relative to a wavelength, these simple expressions are no longer valid. Furthermore, resonators with exaggerated shapes, such as pancake

or deep cavities, have been shown to exhibit more error [41]. These additional errors have not been observed when modeling exaggerated shapes with the impedance translation method.

3.4 Systems of Resonators

In many cases, multiple resonators may be connected in series-parallel configurations to maximize space usage. Regardless of modeling method, the impedance translation formula may be useful in modeling extended systems of resonators.

For example, an arbitrary system of resonators may consist of two Helmholtz resonators in parallel with a length of pipe separating another parallel combination of quarter-wave resonators. In this case, each Helmholtz resonator may be modeled with each acoustic impedance added in parallel. Then, the resultant impedance may be translated using Eq. (3.1) and added in parallel with the acoustic impedance of the remaining quarter-wave resonators.

3.4.1 T-Junctions

Joining any number of acoustic resonators necessitates the use of a T-junction, cross, or similar element. Due to the space constraints associated with the current project, this discussion will involve a detailed treatment of the two-port T-junction. However, the formulations can be generalized to most N-port junctions.

Consider two Helmholtz resonators and a short side branch joined together by a T-junction. In an ideal T-junction, the three branches merge into one well-defined cavity. However, practical T-junctions are slightly larger in diameter than the branches being merged in order to accommodate the outer diameters of each branch. Additionally, physical T-junctions rarely allow each branch to align with each other and create a well-defined cavity. These practical limitations necessitate the addition of a small acoustic mass in each branch to compensate for the extended length and larger

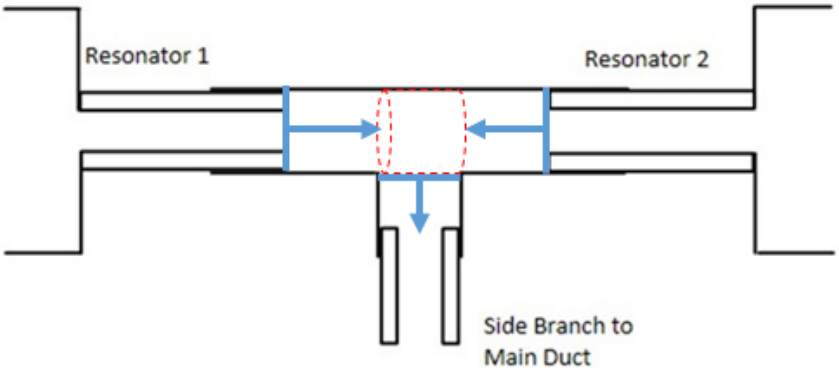

Figure 3.3 Schematic detail of a practical T-junction. The impedance translation over the cross-sectional area of the T-junction is shown in blue and the shared volume is shown in red.

diameter. The added inertance can be accounted for using impedance translation from the physical end of the neck to the beginning of the shared cavity. Figure 3.3 shows a schematic of a practical T-junction. The added mass is modeled as an impedance translation over the region shown in blue, while the shared cavity is shown in red.

Pierce [67] derived the impedance at the output port of a cavity with an arbitrary number of inputs. Assuming the net volume velocity out of the volume is zero and that the pressure is uniform throughout the junction region, he gives the following expression:

$$\frac{1}{Z_{out}} = \sum_{n=1}^{N} \frac{1}{Z_{in,n}} + \frac{jkV}{\rho_0 c}, \tag{3.10}$$

where V is the volume of the junction. For the two resonator and side branch case described above, the impedance from each Helmholtz resonator branch can be inserted into Eq. (3.10) as $Z_{in,n}$ to obtain the impedance Z_{out} looking into the side branch.

3.5 Experimental Comparison of Methods

In order to examine the accuracy of each of the previous methods, various resonators of ideal geometries were constructed and tested. The necks were made from 1 inch and 1-½ inch internal diameter, schedule 40 PVC pipe. Many different lengths were cut to be used as resonator necks and side branches. The cavities were made from 3-¾ inch internal diameter acrylic. A solid plastic cap was machined and fixed to one end of the cavity where necks of each size could be attached. A movable plunger with O-ring seals allowed for the other end to control the volume of the cavity.

The two microphone method [68, 69] was used in a standard 10 cm diameter impedance tube to obtain transmission loss data. The two microphone method employs a pair of microphones to extract the incident and reflected waves at some point in the tube. This separation allows one to compute parameters such as transmission loss, impedance, and absorption coefficients. For the measurements in this study, microphone spacing was chosen to be 0.35 m. This spacing should provide accurate results over a frequency bandwidth of approximately 50 Hz to 400 Hz [70].

A single Helmholtz resonator in parallel with a main duct (see Fig. 3.4) was modeled using each of the methods described in this chapter. The neck was 15.2 cm in length with a 2 cm radius and the cavity was 17.8 cm in length with a 4.8 cm radius. The impedance translation method used Eqs. (2.5)–(2.7) for the junction impedance between the neck and cavity. The element-by-element method utilized the empirical end corrections given by Eq. (2.3) for the neck to cavity transition. The lumped element method used the classical end correction for an infinite baffle. Each method used the empirical end correction from Eq. (2.4) for the end correction due to the side branch configuration. The results in Fig. 3.5 show a comparison of measured transmission loss and each modeling method.

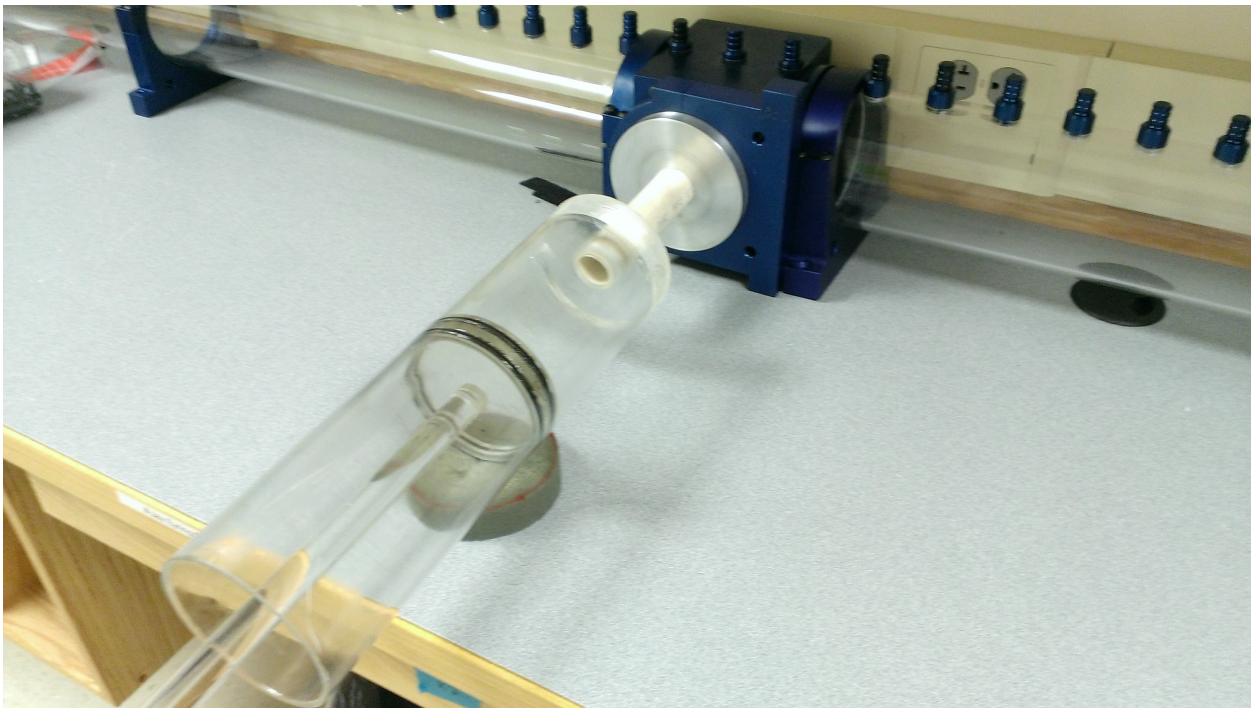

Figure 3.4 Setup of the single resonator side branch

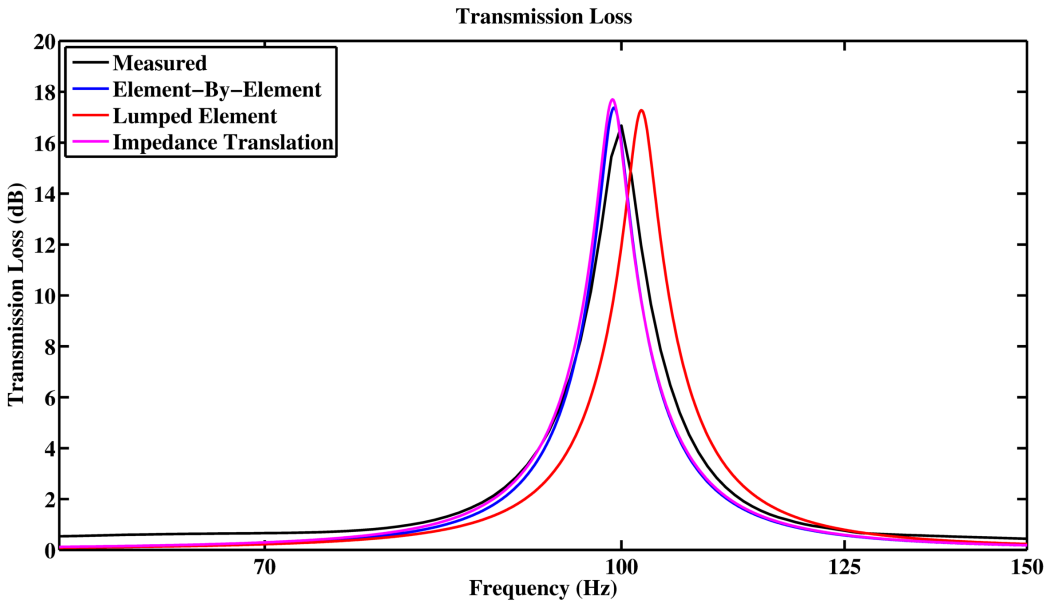

Figure 3.5 Comparison of modeling methods and transmission loss data obtained for a single Helmholtz resonator.

The results in Fig. 3.5 show that the impedance translation and element-by-element methods accurately predict the transmission loss. The data were taken with 1 Hz resolution, which may account for the small discrepancy in magnitude. Even for the simple case, the lumped element method exhibits errors in its prediction.

A dual Helmholtz resonator system—as seen in Fig. 3.6—was also modeled using each of the previous methods. Figure 3.7 shows a detailed schematic of the system under test. An equivalent circuit, shown in Fig. 3.8, was designed to represent the physical resonator system. Relevant dimensions are also given in Table 3.1.

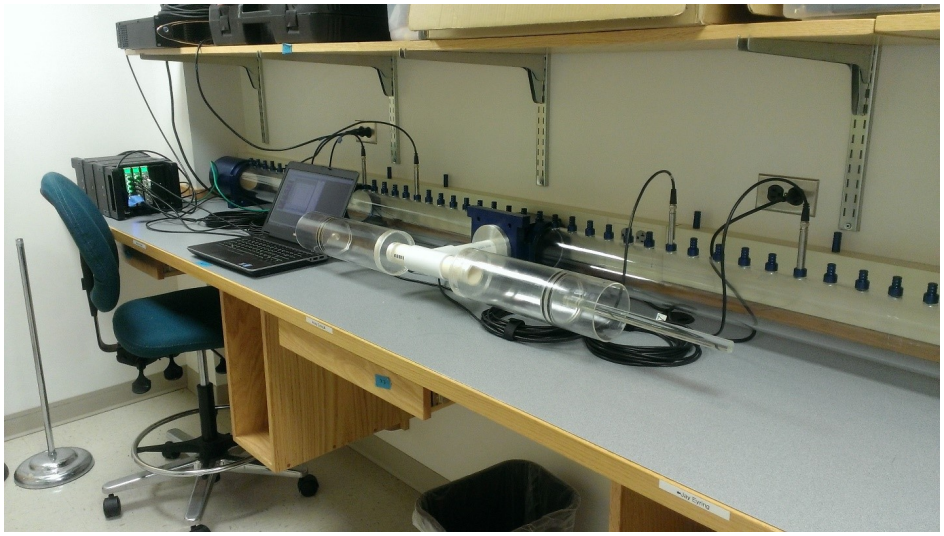

Figure 3.6 Setup of the dual resonator array.

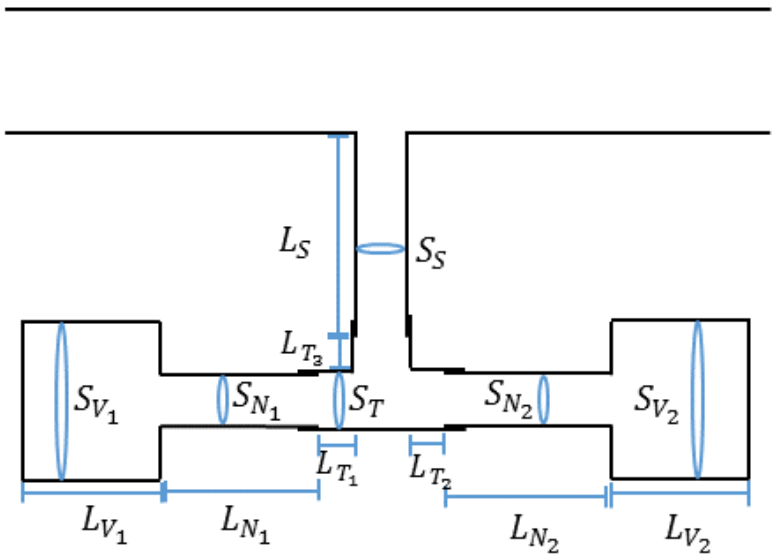

Figure 3.7 Schematic view of dual resonator system with pertinent dimensions.

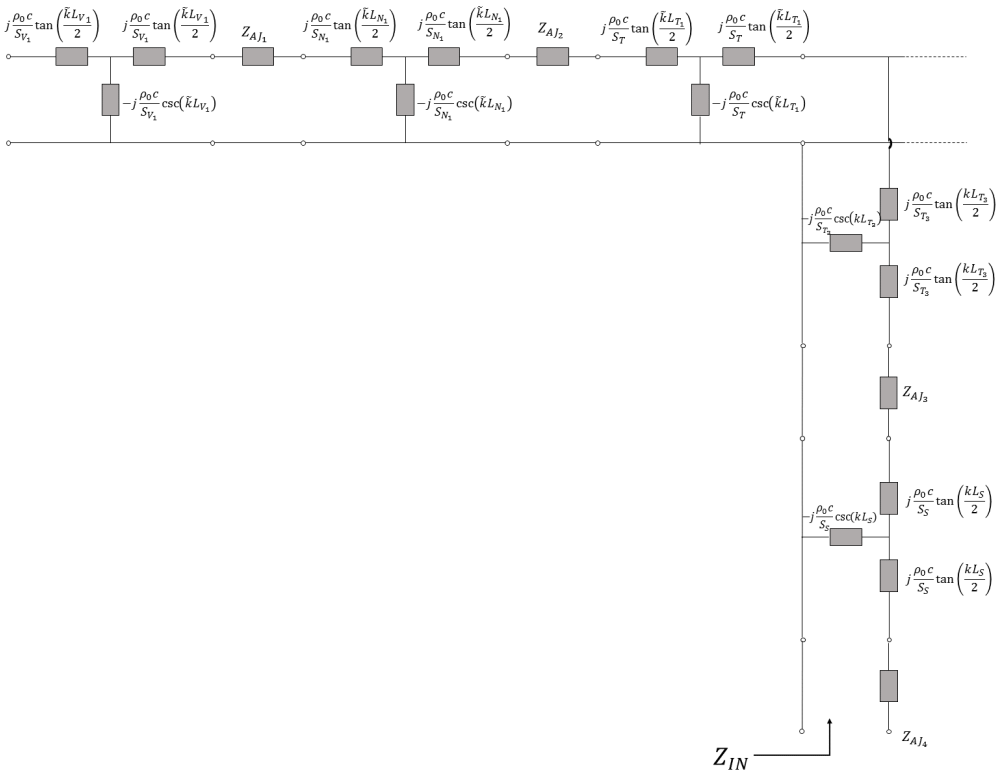

Figure 3.8 Equivalent circuit representation of dual-resonator system. The dots to the right of the circuit represent the branch leading to the second resonator.

Table 3.1 Dimensions of dual-resonator system for transmission loss tests.

Resonator Dimensions				
	L_V (cm)	r_V (cm)	L_N (cm)	r_N (cm)
Resonator 1	19.05	4.75	15.29	2.03
Resonator 2	19.05	4.75	15.27	2.03
T-Junction Dimensions				
	L_T (cm)	r_T (cm)		
Branch 1	1.47	2.42		
Branch 2	1.00	2.42		
Branch 3	1.54	2.42		
Side Branch Dimensions				
	L_S (cm)	r_S (cm)		
Side Branch	15.65	2.03		

The transmission loss data obtained for the system are shown in Fig. 3.9. The differences between each method are more apparent for this more complicated system of resonators. As expected, the lumped element method performs best at low frequencies with decreasing accuracy with increasing frequency. The element-by-element method performs only slightly better than the lumped element method at low frequencies. Higher harmonics also exhibit more accuracy than with the lumped element method. However, since each segment of the system is considered independently, the predictions at higher frequencies are still inadequate.

The impedance translation method shows very little discrepancy for each system resonance. Furthermore, magnitude predictions are more accurate at all frequencies than the other methods. This is primarily due to the inclusion of losses present at the discontinuity that can be added to the frequency-dependent junction impedance.

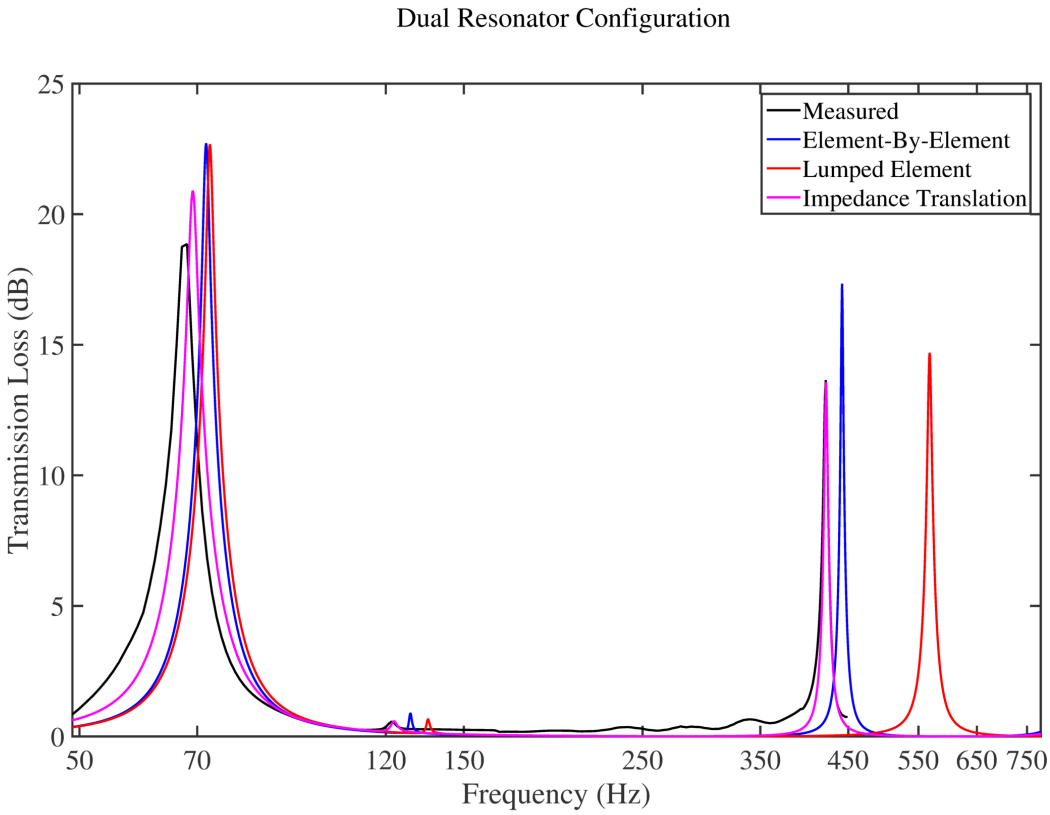

Figure 3.9 Comparison of modeling methods and transmission loss data obtained for a dual Helmholtz resonator system.

3.6 Graphical User Interface

The methods from Chapters 2 and 3 were incorporated in a graphical user interface (GUI) to facilitate predictions of ideal-geometry resonators. The GUI was developed using MATLAB and compiled into a standalone application for easy distribution.

The GUI allows a user to specify characteristics of a Helmholtz resonator and compute its input acoustic impedance. All internal dimensions of a resonator may be input directly into the GUI. Additional options exist for choosing the mounting configuration. The parallel option accounts for the end corrections associated with a resonator mounted as a side branch to a main duct. Likewise, the series option uses the end correction for a resonator at the end of a main duct. The enclosure setting applies the baffled end correction from Eq. (2.1).

The GUI also allows for the addition of flow resistive materials. A user may select from a library of materials and specify thickness. The cross-sectional area is automatically computed from the neck dimensions chosen by the user. Once each property of the resonator is determined, the GUI calculates and displays the input acoustic impedance for the Helmholtz resonator as well as the resonance frequency. An example is shown in Fig. 3.10.

The calculations are performed based on the impedance translation theorem and frequency-dependent end corrections. Internal resistance is also accounted for in the predictions. This tool allows engineers to quickly and accurately determine the input acoustic impedance of a prototype Helmholtz resonator in various configurations.

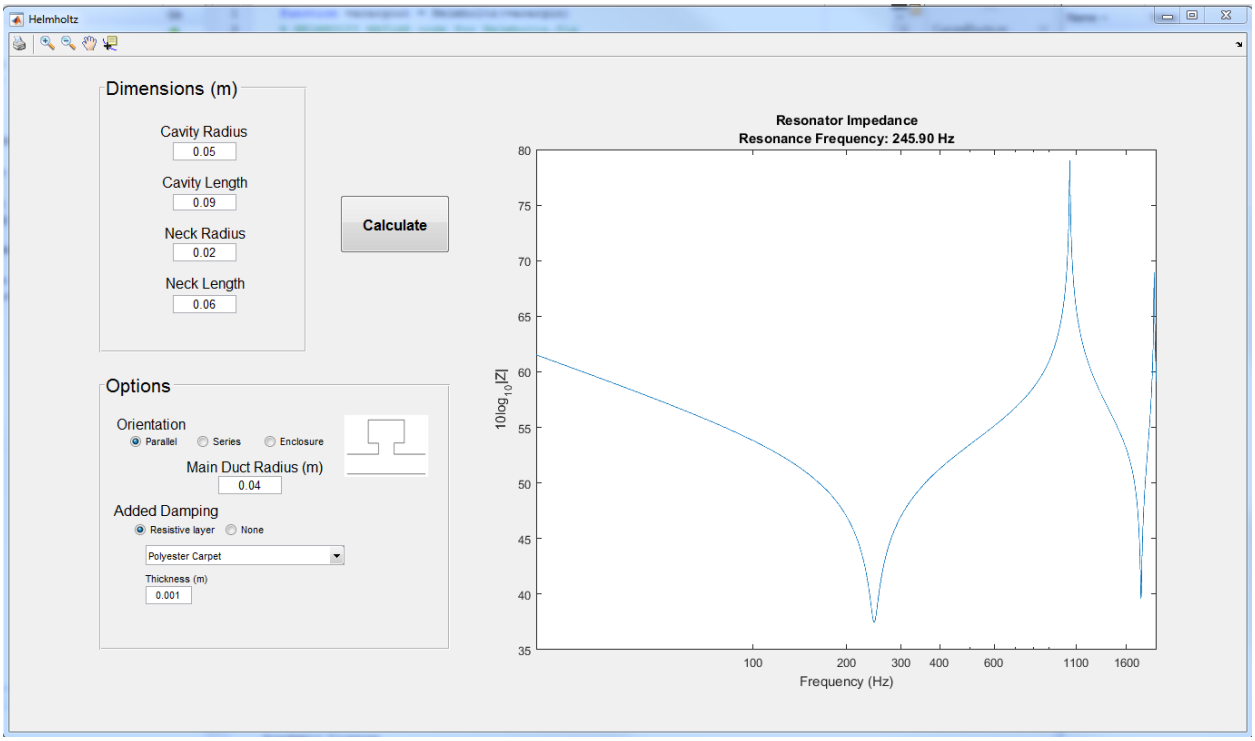

Figure 3.10 Screen capture from graphical user interface for designing damped Helmholtz resonators of ideal geometries.

Chapter 4

Modeling of Resonators with Nonideal Geometries

In engineering applications, space constraints often dictate the geometries present in the final product. Therefore, it is important to accurately predict the effect of any nonideal geometries in a given resonator system. This chapter introduces two such geometries and gives analytical expressions for modeling them. Measured results are used to validate the theoretical formulations.

4.1 Helmholtz Resonators with Tapered Necks

The traditional resonator neck of constant cross-sectional area can be modified to change in area with increasing length. The current research focuses on modeling tapers of constant slope, although other methods exist for approximating the acoustic responses of other flare types [71–73].

4.1.1 Theoretical Treatment

Using the information provided in previous chapters, one can qualitatively predict the effects of neck tapering. The basic expression given in Eq. (3.9) shows a direct relationship between resonance frequency and cross-sectional area. For a neck that increases as a function of length, one would predict an increased resonance frequency relative to a neck with constant cross-sectional area and radius equal to the smallest part of the taper. Likewise, thermoviscous losses that occur near tube walls are inversely proportional to tube radius. Therefore, a tapered neck would suggest decreased damping at resonance when compared to a straight neck with constant radius equal to the inlet.

Tang [44] developed theoretical expressions for the acoustic impedance of a Helmholtz resonator with a tapered neck. His derivations assume plane-wave propagation in order to derive an approximate analytical solution within the taper.

Consider a Helmholtz resonator with a tapered neck as shown in Fig. 4.1. The neck radius, r_i, flares over a length L to a larger radius, r_0, at the inlet to the cavity such that the slope is given by $m = (r_0 - r_i)/L$. Following the derivation given by Tang, the ordinary differential equation for pressure can be written as

$$\frac{\mathrm{d}^2 p}{\mathrm{d}x^2} + \frac{2m}{mx + r_i}\frac{\mathrm{d}p}{\mathrm{d}x} + k^2 p = 0. \tag{4.1}$$

The solution for p may be found using standard techniques and the particle velocity u can be determined from Euler's equation. Tang defined the normalized specific acoustic impedance at the inlet to the resonator cavity as

$$z_0 = \frac{p}{\rho_0 c u}\bigg|_{x=L} = \frac{\pi r_0^2}{jkV} \tag{4.2}$$

where V is the volume of the cavity.

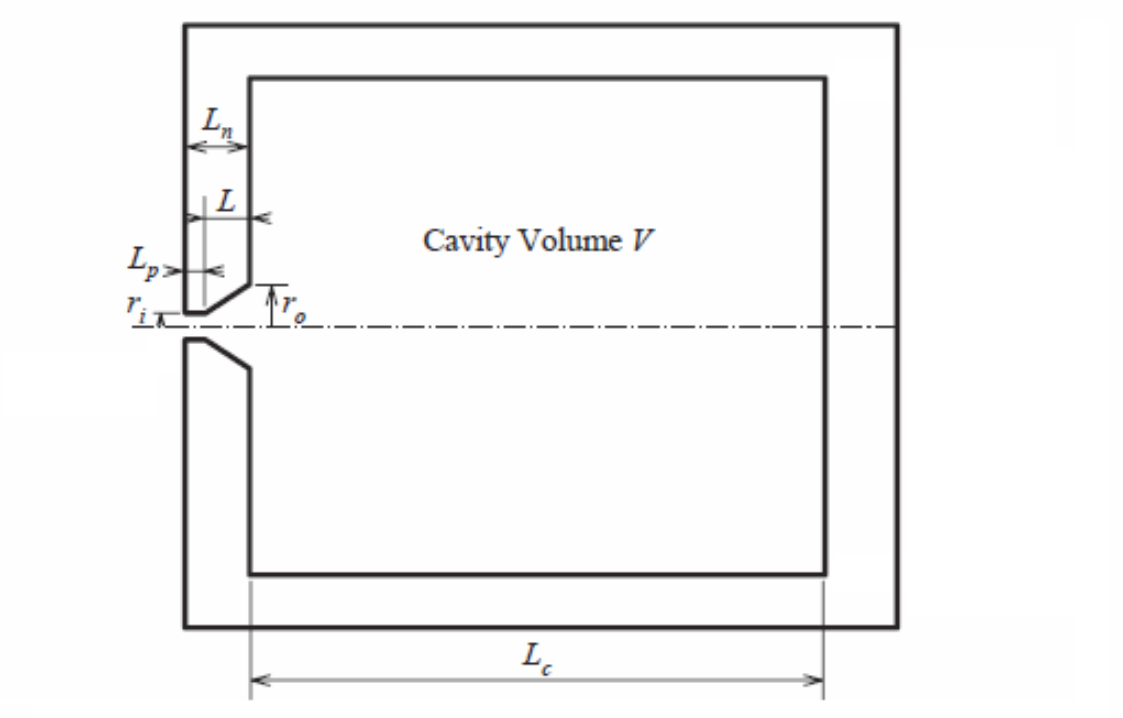

Figure 4.1 Schematic of Helmholtz resonator with tapered neck [44].

The specific acoustic impedance at the inlet of the tapered neck can then be found, after Tang, as

$$z_i = \frac{k^2 r_i r_0 z_0 + (jk^2 r_i r_0 - k r_i m z_0)\tan kL}{k^2 r_i r_0 - jkm^2 L z_0 + (k r_0 m + jm^2 z_0 + jk^2 r_i r_0 z_0)\tan kL}, \tag{4.3}$$

which can then be translated via Eq. (3.1) over any remaining length of constant cross-sectional area.

Thermoviscous losses at tube walls become more difficult to determine analytically because of the changing cross section. Tang showed that the pressure loss associated with incompressible flow through an enlargement is proportional to the squared velocity [44, 74]. If the wavelength is much larger than the dimensions of the resonator, the resistive impedance is expected to be proportional to r_i^2/r_0^2. This approximation predicts a reduction in resistance due to the tapered neck, which in turn suggests higher absorption at resonance.

Tang [44] also gives a simple expression for the resonance frequency of a Helmholtz resonator with a tapered neck. The expression is obtained by solving a simplified, long-wavelength version of Eq. (4.3) and is given here to provide intuition into the changes induced by tapering:

$$f_0 = \frac{c}{2\pi}\sqrt{\frac{\pi r_i^2}{LV} + \frac{m\pi r_i}{V}}. \tag{4.4}$$

This result confirms the qualitative behavior predicted at the beginning of the current section. The simplified derivation shows an increased resonance frequency dependent upon the slope of the taper.

4.1.2 Comparison with Measured Results

In order to validate the theoretical model, a tapered neck was constructed for the existing adjustable cavity. The taper was machined from PVC using a lathe in conjunction with a mounting disc. It consisted of a straight neck of constant cross section and a taper of constant slope. The straight neck had a 1 inch internal diameter over a length of approximately ½ inch. The tapered section

had a length of 3 inches and expanded from an internal diameter of 1 to 1-½ inches with a constant slope. Figure 4.2 shows the tapered neck with an overlay of the internal topography.

Figure 4.2 Fabricated tapered neck with overlay of internal dimensions.

The acoustic impedance for the tapered Helmholtz resonator was obtained from the two microphone method. The resonator was mounted at the end of the plane wave tube so acoustic impedance could be measured directly. In this configuration, the acoustic impedance at the plane-wave tube termination consisted of both the solid aluminum termination seen in Fig. 4.2 and the smaller opening to the resonator. Therefore, the acoustic impedance of an identical aluminum termination was measured without an opening, which was then used to extract the acoustic impedance for only the cross-sectional area of the opening. Since acoustic impedance measurements offered a more direct comparison to modeled results, all further measurements were conducted with the resonator as a termination to the plane-wave tube.

Two Helmholtz resonators with straight necks of 1 inch and 1-½ inches diameter were also measured to compare their response to the tapered neck. While the three cross-sectional areas

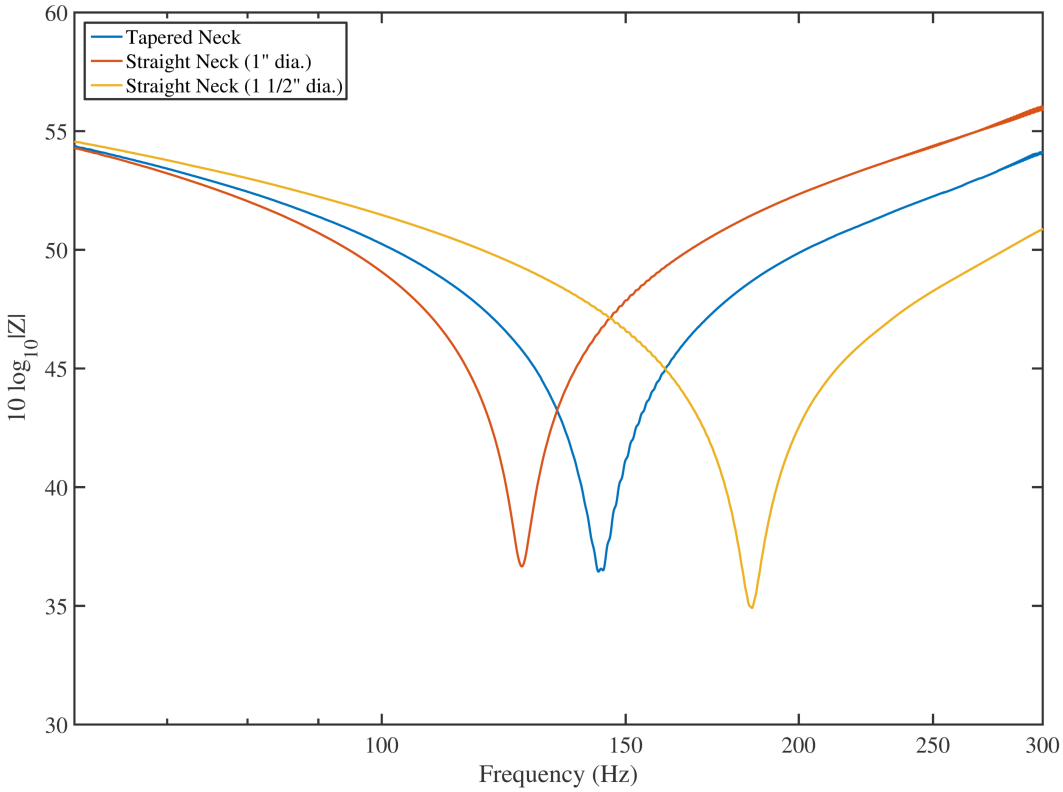

Figure 4.3 Empirical comparison of straight and tapered Helmholtz resonators.

were different between each case, the overall length and volume were unchanged between tests.

Figure 4.3 shows the effect of a neck taper compared to the two traditional Helmholtz resonators. As predicted in the discussion above, the measured resonance frequency of the tapered neck falls between the resonance frequencies of the two resonators with straight necks. The predicted increase in efficiency is seen as a slightly lower minimum in the acoustic impedance measurements. The increase in efficiency was observed to be very minor for the present measurements.

The formulations given by Tang in Eqs. (4.2)–(4.3) were adapted from normalized specific acoustic impedance to acoustic impedance for comparison. While the qualitative effects are present, the simplified formulation given by Tang in Eq. (4.3) exhibits some disagreement with the actual results. Figure 4.4 shows that the simplified expression underestimates the measured response by

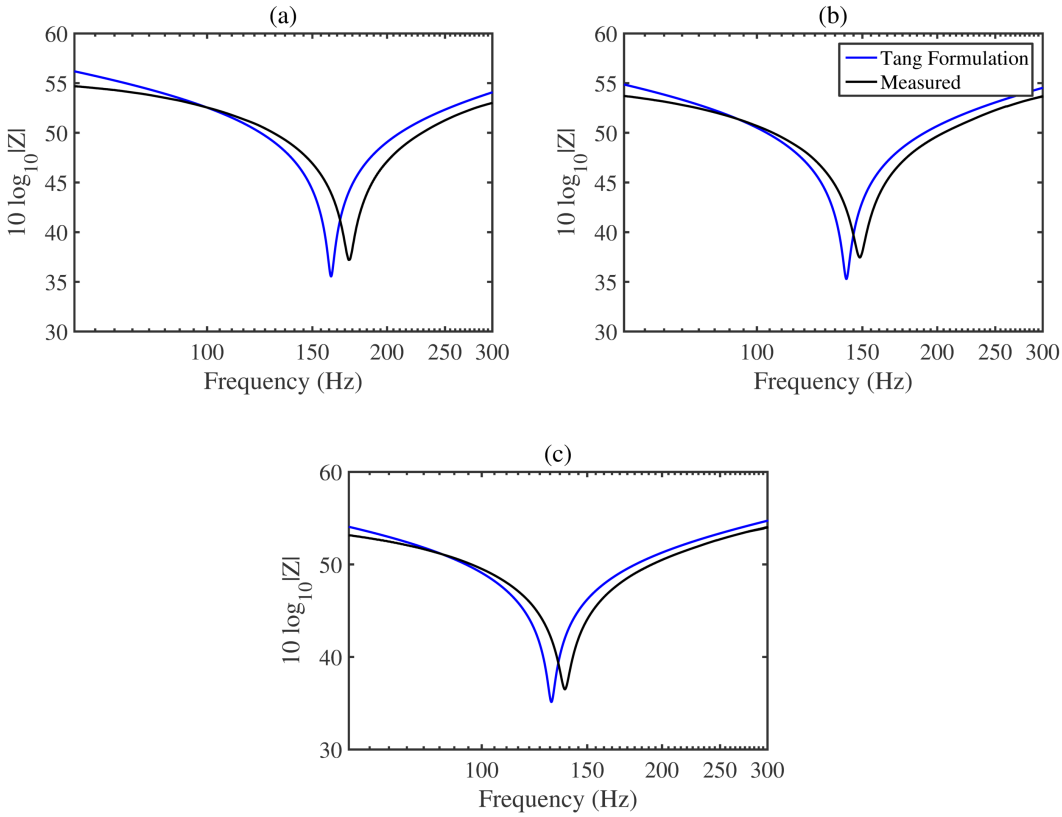

Figure 4.4 Comparison of measured acoustic impedance and formulations by Tang for different cavity lengths: (a) 9.8 cm, (b) 13 cm, and (c) 15.2 cm.

up to 11 Hz.

In order to correct for this discrepancy, several modifications were made to the original formulation. First, more accurate end corrections were considered. Tang used the simplified end correction from Eq. (2.1) on each side of the tapered neck. The frequency-dependent end corrections expressed in Eqs. (2.5)–(2.7) were applied at the mouth of the resonator and at the interface between r_0 and the cavity.

Tang also considers the cavity as a lumped element compliance. As discussed previously, this assumption ignores the mass-like impedance that is present within the cavity. Therefore, an impedance translation was performed over the length of the cavity and inserted into Eq. (4.3) as z_0.

As shown in Fig. 4.5, the modifications improve the predictions of acoustic impedance in a tapered neck. The higher-order approximations allow the resonance frequency to be predicted within 1 Hz.

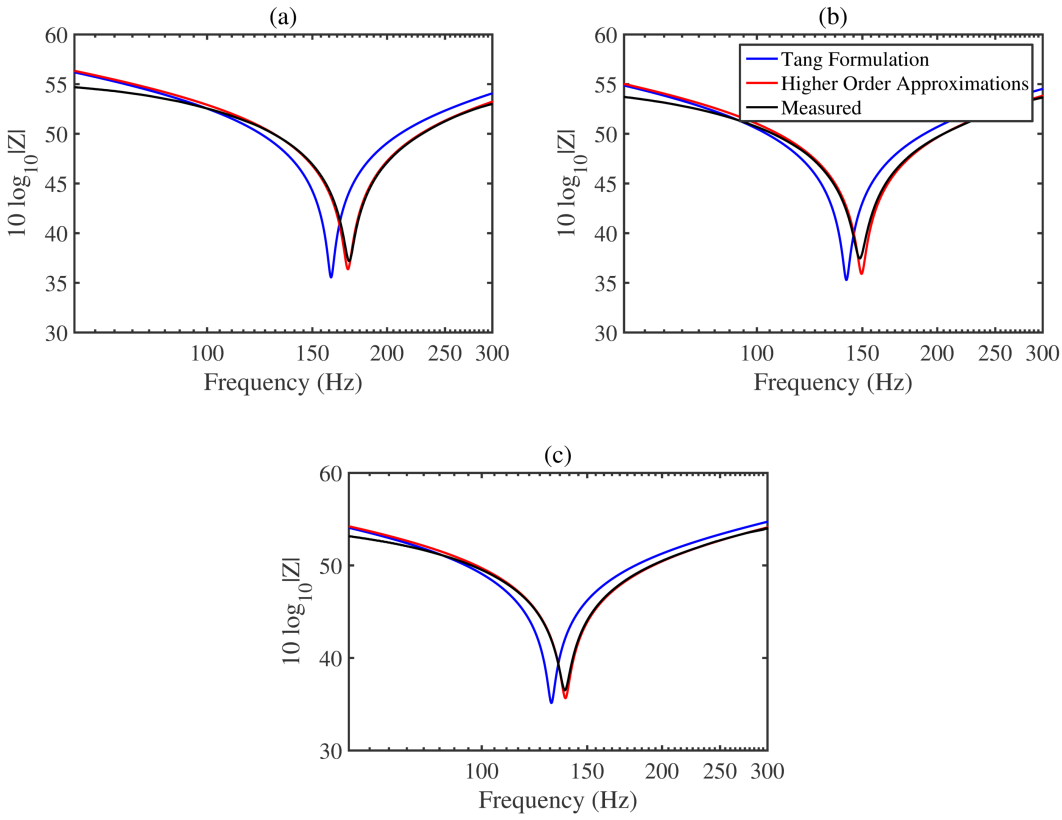

Figure 4.5 Comparison of acoustic impedance and modified theory for different cavity lengths: (a) 9.8 cm, (b) 13 cm, and (c) 15.2 cm.

4.2 Helmholtz Resonators with Curved Necks

While many researchers have explored the acoustic properties of curved waveguides for application in HVAC ducts, automotive exhaust systems, and musical instruments, research regarding Helmholtz resonators with curved necks remains scarce. Indeed, common practice is to consider the length of a bend at its centerline and model the system as if it were straight [46]. However, such simplification is likely to introduce unacceptable errors as frequency and complexity increases.

4.2.1 Theoretical Treatment

The propagation of sound in curved ducts differs from propagation in straight ducts. A plane wave impinging on a curve will experience a discontinuity at the inlet. Within the region of the bend, plane waves no longer propagate and wave velocity is frequency dependent or dispersive [46, 75]. The sound field contained within the bend is characterized by modes not found in straight sections, which many authors refer to as radial and tangential modes [50, 76]. These modes become evanescent once the wave has exited the bend and the result is a plane wave of smaller amplitude [48].

Cummings [46] examined the response of curved ducts with rectangular cross section. He solved an exact solution to the wave equation within the bend using boundary conditions defined in cylindrical coordinates. The analytical expression is similar to the solution of an annular straight duct. Although an exact solution for the impedance of a curved duct was found, Cummings made simplifying assumptions to reduce computational cost. He found reasonable agreement at very low frequencies by simply correcting for the length of the bend at its centerline as follows:

$$\zeta_B = j \cot k(L_m + l), \tag{4.5}$$

where ζ_B is the normalized acoustic impedance, L_m is the median length of the bend, and l is the length of straight section following the bend. While other expressions have since been developed for rectangular ducts [77, 78], the present research is most interested in the impedance for curved

ducts of circular cross section.

Sound propagation in circular curves is more difficult to express analytically than the rectangular case. In order to accurately define the boundary conditions in a curved duct of circular cross section, toroidal coordinates must be used. Unfortunately, the wave equation is not separable in toroidal coordinates, which precludes analysis by conventional means [46].

While closed-form solutions have not yet been developed, Cummings [46] proposed two potential approximations for circular section ducts. First, due to the similarities between the measured pressure fields in bends of rectangular and circular ducts, he proposed use of an equivalent rectangular bend with cross-sectional area equal to that of the circular bend under consideration. This approximation shows fair agreement for low frequencies, but is recommended only as a design guide for rough estimations. Second, Cummings visualized the circular section as a series of slices of rectangular ducts in the plane of the bend. He proposed an averaging process over each slice, but gave no formal derivation of this approximation.

Keefe and Benade [79] adapted Cummings' second approximation for impedance calculations of musical instruments. They considered one cross section in the plane perpendicular to the direction of acoustic propagation in the bend. This cross section was then subdivided into a series of rectangular slices of infinitesimal height. The slices were calculated independent from one another, i.e., pressure variations in the vertical z direction and shear were assumed to be negligible. With these assumptions, the approximate response is the parallel combination of the inertance and shunted compliance of each slice.

The compliance per unit length for each slice can then be written as

$$C_i = S/\rho_0 c^2, \tag{4.6}$$

where

$$S = (R_2 - R_1)\mathrm{d}z \tag{4.7}$$

and where R_1 and R_2 represent the inner and outer radii of curvature of the bend, respectively, as

seen in Fig. 4.6. Each slice is then summed in parallel to obtain the total compliance per unit length as follows:

$$C_t = \sum_i C_i = \frac{\pi r_0^2}{\rho_0 c^2}, \tag{4.8}$$

where r_0 is the radius of the pipe. It is interesting to note that the compliance is simply the ratio of cross-sectional area and bulk modulus. This compliance is equal to the compliance of a straight pipe of the same cross section [79].

In order to express the inertance of each cross section, Keefe and Benade defined a bend parameter B such that

$$B = \frac{r_0}{R_m} \tag{4.9}$$

where r_0 is the radius of the pipe and R_m is the mean radius of curvature as shown in Fig. 4.6. This is used to calculate the position of each infinitesimal slice within the circular cross section as follows:

$$a = \frac{1 + B[1 - (z/r_0)^2]^{1/2}}{1 - B[1 - (z/r_0)^2]^{1/2}}. \tag{4.10}$$

The inertance per unit length of each slice can then be written as

$$L_i = \frac{\rho_0}{R_m \mathrm{d}z \ln a}. \tag{4.11}$$

Each slice is summed in parallel to obtain the total inertance per unit length as follows:

$$\frac{1}{L_t} = \sum_i \frac{1}{L_i} = \frac{R_m}{\rho_0} \int_{-r_0}^{r_0} \ln a \, \mathrm{d}z. \tag{4.12}$$

Once the compliance and inertance are summed over each slice, the acoustic impedance per unit length can be computed as

$$Z_b = \sqrt{\frac{L_t}{C_t}}, \tag{4.13}$$

which can be considered as a characteristic bend impedance over any length of constant radius of curvature. This is analogous to the characteristic acoustic impedance $\rho_0 c/S$ found by considering

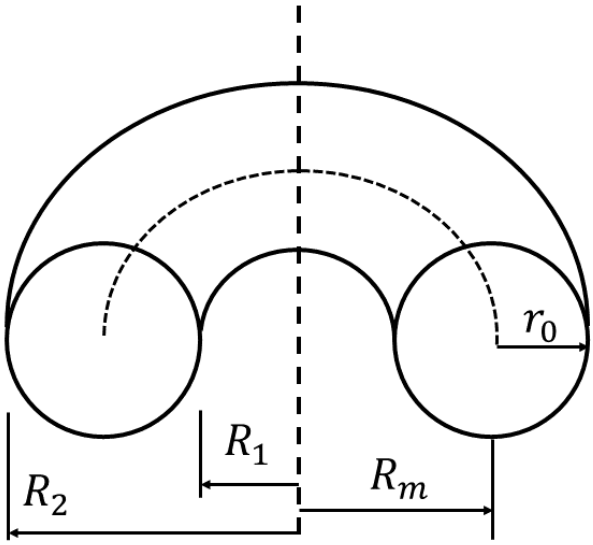

Figure 4.6 Schematic of relevant dimensions for a bend of circular cross-sectional area.

the impedance of a semi-infinite straight duct. Therefore, if one substitutes the characteristic bend impedance from Eq. (4.13) for the characteristic impedance in Eq. (3.1), it is possible to obtain an approximate expression for the impedance translation over any length of constant cross-sectional area and constant radius of curvature. This approximation is written as follows:

$$Z_{A0,\text{bend}} = Z_b \frac{\dfrac{Z_{AL}}{Z_b} + j \tan \tilde{k} L_m}{1 + j \dfrac{Z_{AL}}{Z_b} \tan \tilde{k} L_m}. \tag{4.14}$$

The result allows higher-order effects to be preserved throughout the entire system. It can be used to model resonator systems with curved sections as well as Helmholtz resonators with curved necks. Furthermore, the equivalent circuit representation of the impedance translation theorem can be rewritten to include the characteristic bend impedance. Figure 4.7 shows the equivalent T-network for the impedance translation over a curve of circular cross section.

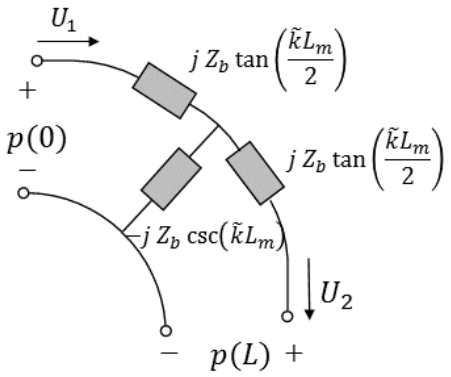

Figure 4.7 Equivalent T-network for representing the impedance translation over a curve of circular cross-sectional area.

4.2.2 Comparison with Measured Results

Validation of the theory for curved circular ducts presented in the previous section was conducted with acoustic measurements of curved PVC pipes. The two-microphone method was used to obtain the acoustic impedance of a single, curved-neck Helmholtz resonator. The neck consisted of two short straight sections of 7.65 cm on either side of three different bends: a short 60° bend, a short 90° bend, and a long 90° bend. The cavity length was 19.05 cm for each of the tests. Figure 4.8 shows the measurement setup with the short 60°. Table 4.1 shows the dimensions of each bend.

The integral approximation from Keefe and Benade was used to predict the input impedance

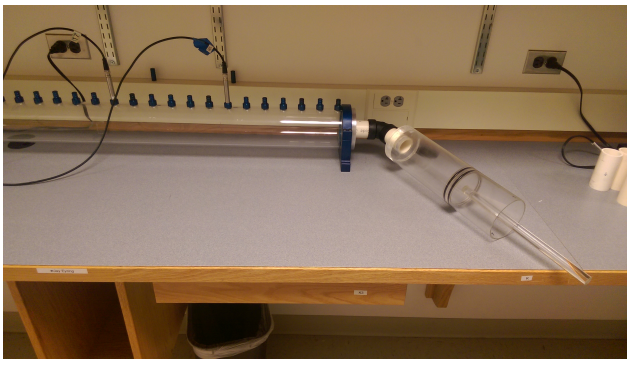

Figure 4.8 Measurement setup for Helmholtz resonator with curved neck.

Table 4.1 Dimensions for each PVC bend used in measurements.

	Inner Radius of Curvature (cm)	Outer Radius of Curvature (cm)	Mean Arc Length (cm)
60°	1.33	5.14	3.39
90° (Short)	1.71	5.43	5.61
90° (Long)	4.39	7.90	9.65

and absorption coefficient of the curved Helmholtz resonator. Figure 4.9 shows the equivalent circuit representation of the resonator. The lumped-element method was also used with the assumption of an equivalent straight neck corresponding to the length of the curve at its centerline.

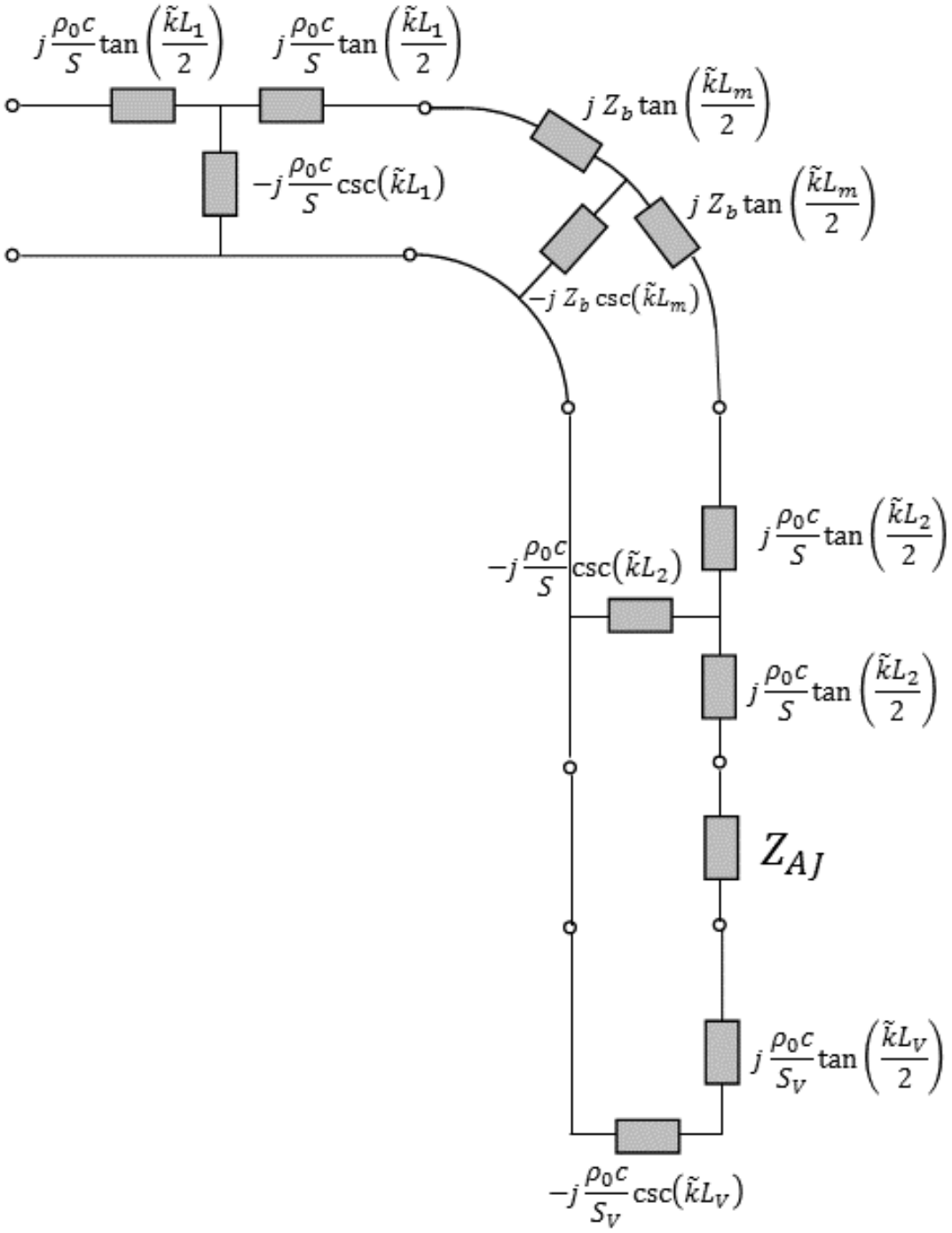

Figure 4.9 Equivalent circuit representation of curved Helmholtz resonator.

Figure 4.10 shows comparisons of measured acoustic impedances and the associated theoretical predictions. The modified impedance translation method predicts the lowest resonance frequency (dip) within 0.5 Hz for each bend and the second resonance frequency within 1 Hz for the modified impedance translation method. The lumped-element method gives only the lowest resonance and overestimates the frequency by up to 6 Hz. In this simple case, the lumped-element approximation with an assumed straight neck shows relatively large discrepancies from measurements.

The measured results show an antiresonance (peak) that does not agree with the modified impedance translation. These discrepancies are only partially attributed to poor coherence due to the strong reflection created at antiresonance and require further investigation. However, for the

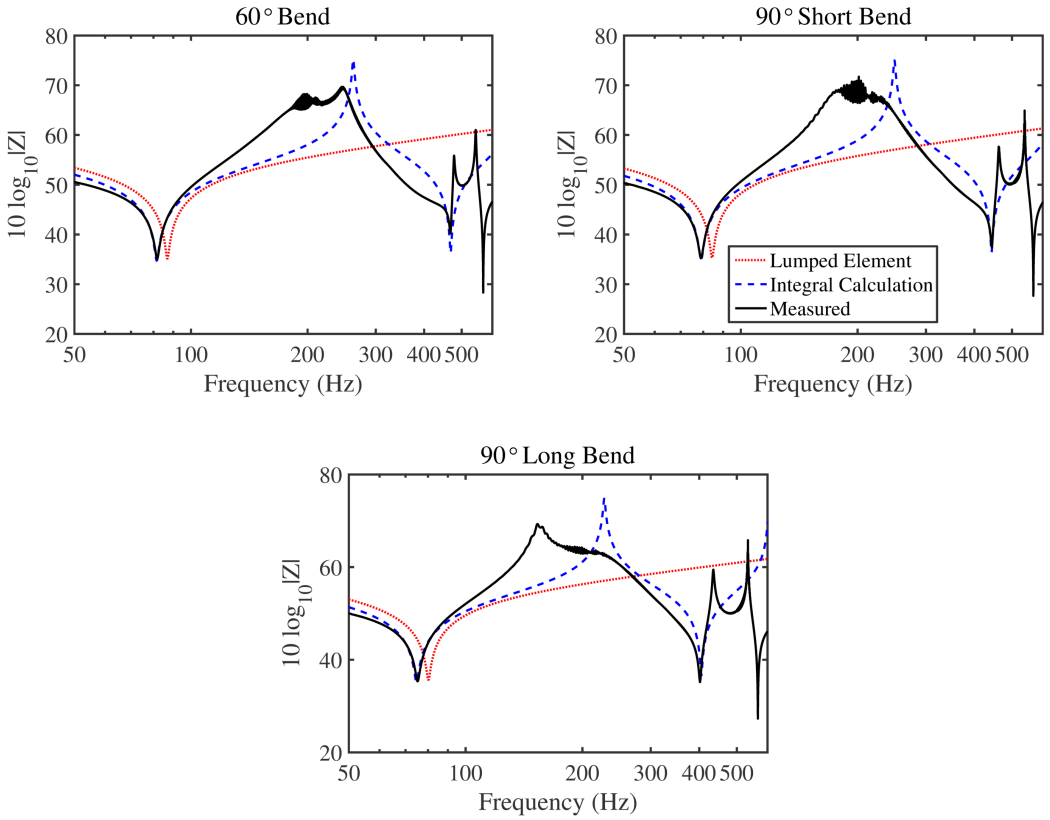

Figure 4.10 Comparisons of measured and theoretical acoustic impedances for a Helmholtz resonator with various curved necks.

purposes of this research, the accurate prediction of system resonances is most important.

In order to further test the accuracy of the impedance translation method, an arbitrary system of curved resonators was fabricated. As seen in Fig. 4.11, the system included the parallel combination of bends with various angles and lengths. Table 4.2 contains the relevant dimensions for this system.

Figure 4.12 shows the measurement results. Even at low frequencies, the lumped-element method does not accurately predict the response of a system with the present complexity. It overestimated the resonance frequency by 9.8 Hz. In contrast, the modified impedance translation

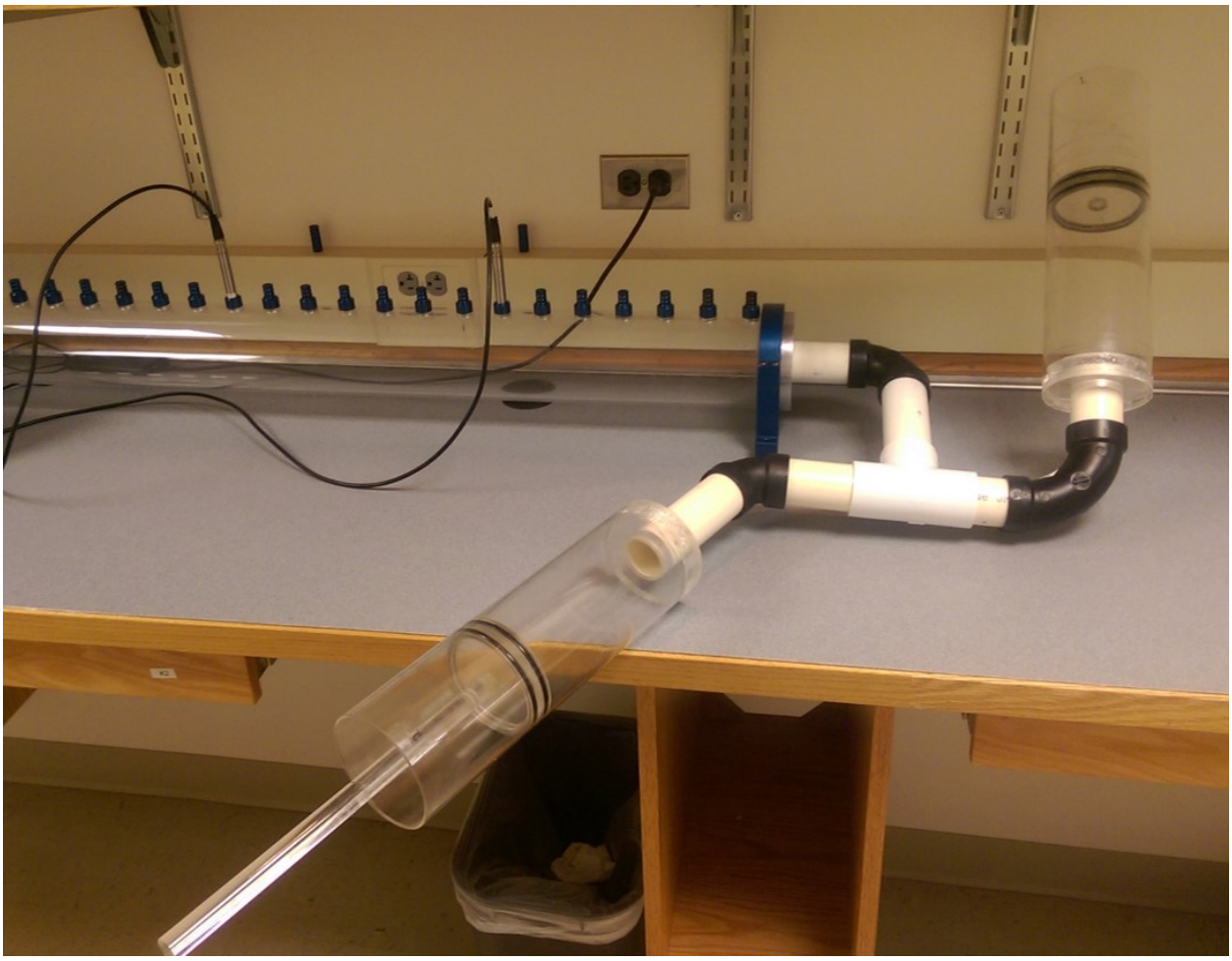

Figure 4.11 Complex system of curved resonators used for model comparisons.

Table 4.2 Dimensions of curved-resonator system for acoustic impedance tests. Subscripts 1 and 2 indicate dimensions of elements before and after a bend, respectively. Bend angles are given as a reference to dimensions given in Table 4.1.

Resonator Dimensions						
	L_V (cm)	r_V (cm)	L_{N_1} (cm)	Bend angle	L_{N_2} (cm)	r_N (cm)
Resonator 1	19.05	4.79	15.62	60°	10.24	2.01
Resonator 2	19.05	4.79	7.98	90° (Long)	7.67	2.01

T-Junction Dimensions		
	L_T (cm)	r_T (cm)
Branch 1	1.47	2.42
Branch 2	1.00	2.42
Branch 3	1.54	2.42

Side Branch Dimensions				
	r_S (cm)	L_{S_1} (cm)	Bend Angle	L_{S_2}
Side Branch	2.01	15.34	90° (Short)	10.22

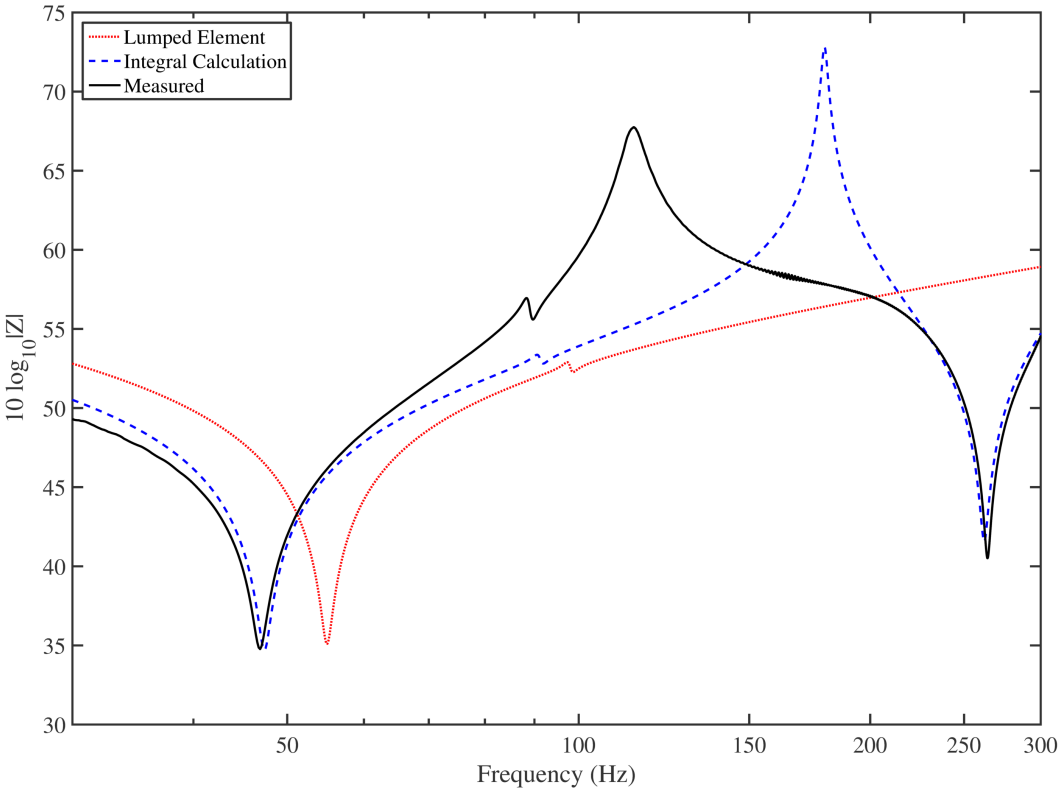

Figure 4.12 Comparison of measured and theoretical absorption coefficients for a complex system of Helmholtz resonators with curved necks

method gives relatively accurate resonance results over all measured frequencies. Both resonances are predicted to within 1 Hz. The data shown in Fig. 4.10 and Fig. 4.12 show the inaccuracies associated with current engineering methods for predicting the responses of curved-neck resonators.

Chapter 5

Resonator-Enclosure Coupling

Acoustic resonators offer a powerful means of controlling unwanted tonal noise in an enclosure. When the tonal noise corresponds to a mode of the enclosure, a resonator can mitigate some of the resonance added by the enclosure. However, theoretical and practical limitations must be considered for maximum absorption to occur. The present chapter will explore the key mechanisms for attenuation in an enclosure due to a coupled resonator or system of resonators.

5.1 Theoretical Treatment

The response of a resonator coupled to an enclosure is somewhat analogous to a tuned mass damper for mechanical systems. Consider a damped mass-spring oscillator with a strong unwanted resonance. If another mass-spring system of similar resonance frequency is attached to the original, it is possible to transfer energy to the new system instead. In this case, a single-degree-of-freedom system becomes a two-degree-of-freedom system. Instead of one strong resonance, two resonances are created at different frequencies.

The coupling between the acoustic modes of an enclosure and a resonator system, however, complicates the analogy given above. First, the input impedance of the resonator system represents

a very localized region within the enclosure. Therefore, resonator placement becomes important in the coupled system. Second, internal damping greatly affects the amount of energy that flows into and is dissipated by the system of resonators. Last, the relative volumes of resonator and enclosure cavities control how much energy can be removed from the enclosure, stored, and dissipated by the resonators.

5.1.1 Resonator Placement

The geometries and boundary conditions of an enclosure give rise to self-reinforcing standing waves at resonance frequencies. At low frequencies and for minimal damping, these resonances are typically narrow and spaced far apart in frequency. As frequency increases, modal density also increases.

Higher frequencies also give rise to distinct mode types. When a mode involves only reflections of sound waves between two parallel walls, it is referred to as an axial mode. Tangential and oblique modes involve reflections from four and six walls, respectively. While any mode type can exist at any frequency, it is most common to see axial modes at low frequencies. Tangential and oblique modes tend to become more prevalent as frequency increases.

For the present research, modal coupling between a single, distinct room mode and the resonator system will be examined. This matches the physical nature of the problem and allows coupling effects to be considered independently of other enclosure and resonator modes.

The placement of a resonator system relative to the acoustic modes of an enclosure will dictate much of the possible absorption. According to Cummings [53], the influence of a resonator system is greatest when it is positioned at a pressure antinode for a given mode. Furthermore, the effect is seen to be greater for oblique and tangential modes than for axial modes [52].

An enclosure was modeled in COMSOL to obtain the shape of the first several acoustic modes. The model assumed infinitely rigid boundaries for each wall. The floor measured 0.95×1.2 m and

the overall height was 1.49 m. The ceiling was 0.95 × 0.92 m, such that one wall had a gradual slant. Figure 5.1 shows the modeled enclosure as displayed in COMSOL.

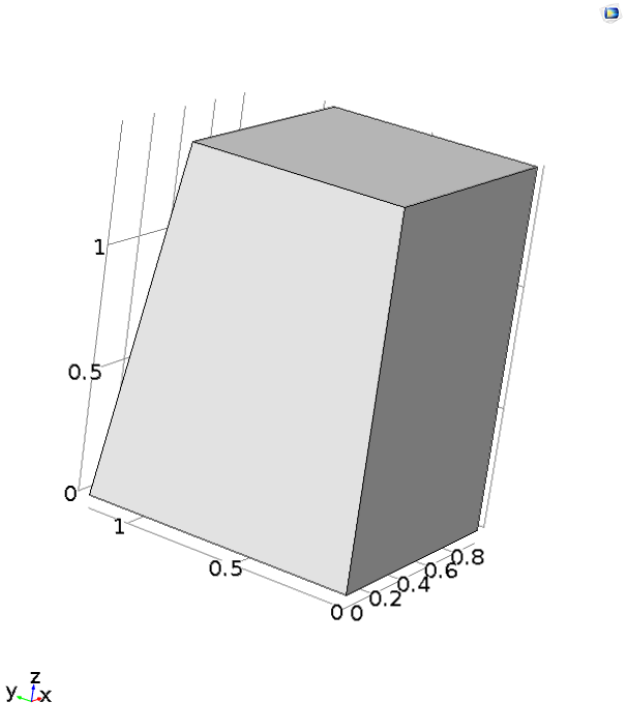

Figure 5.1 COMSOL model of enclosure under test.

The COMSOL acoustics module was used to determine the eigenfrequencies and eigenmodes of the three-dimensional enclosure. Temperature and pressure were taken to be standard local values. The first four acoustic modes of the enclosure obtained from COMSOL are shown in Fig. 5.2.

The overall mode shapes for the test enclosure are similar to those of a rectangular room. The lowest three modes are very close to axial modes, while the fourth mode is a tangential mode. The separation between the first and second modes is 45 Hz, suggesting that the first mode may be considered independently of each of the succeeding modes.

Given the calculated mode shapes and the discussion above, favorable coupling with the first mode could be achieved by placing the resonator system anywhere on top of the enclosure. In

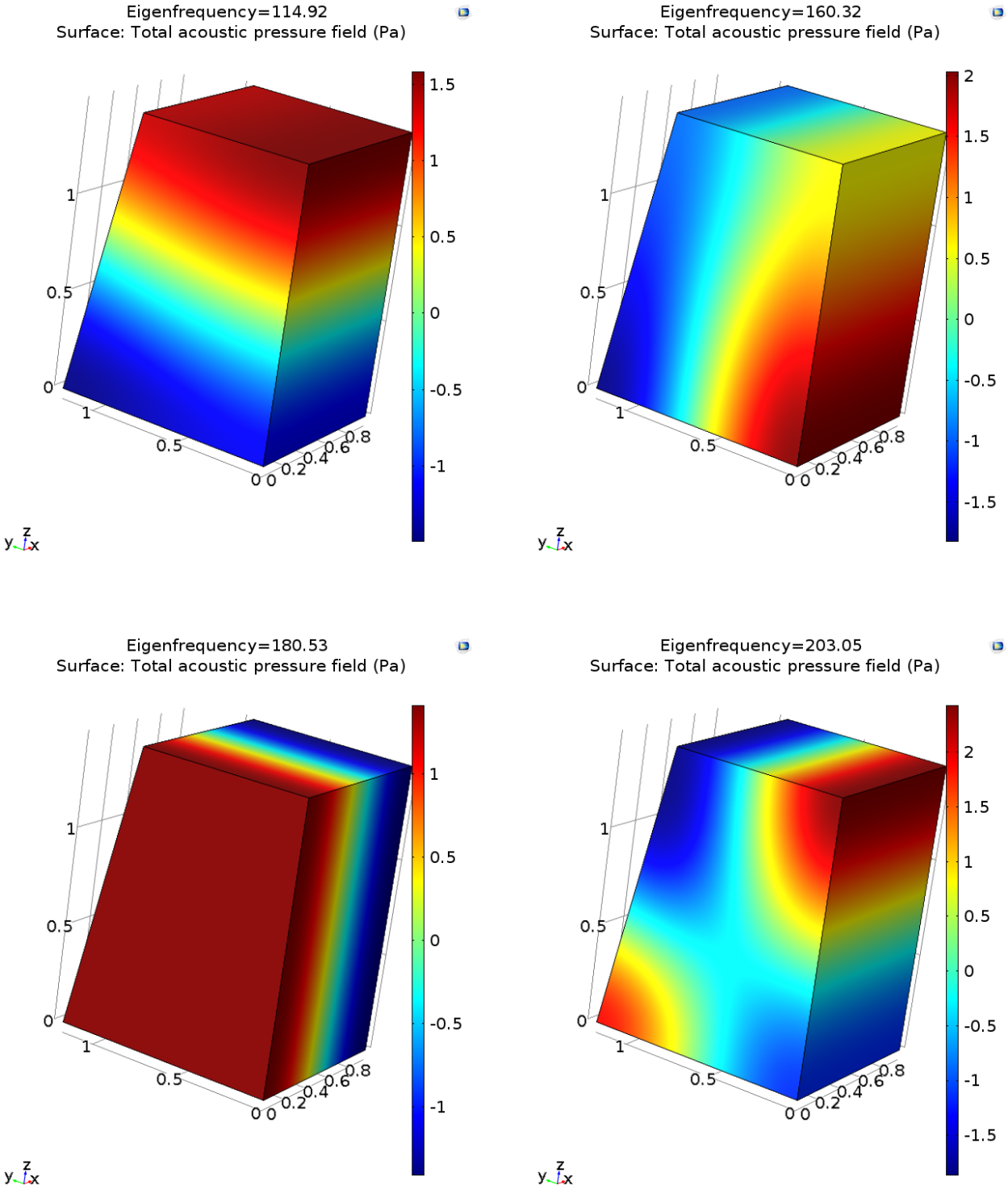

Figure 5.2 First four acoustic pressure modes of COMSOL enclosure model.

order to ensure that the system does not fall on nodal lines from any of the first four modes, the resonator system should not be placed near the centerline of either ceiling dimension.

5.1.2 Damping

Another important factor for maximizing absorption is the amount of damping within the resonator system. As with the tuned-mass damper, the coupling between a resonator-enclosure system introduces new modes of oscillation. When a resonator is tuned to the original enclosure resonance, Fahy [52] found that the energy is split into two resonance on either side of the original frequency.

In this regard, damping can control the dissipation of energy at the original enclosure mode as well as the two closely-spaced, coupled modes. As stated in Chapter 2, resistance can broaden the absorption bandwidth at the cost of efficient dissipation at resonance. This damping comes from thermoviscous losses at tube walls as well as from any facings installed at the resonator mouth or absorptive material placed in the neck or cavity.

For the coupled system, damping must be carefully chosen according to the application. For invariant, narrowband noise at the original enclosure mode, the two coupled peaks may not present a problem. However, given the small spectral variations present in most vehicle interiors, controlling each mode becomes important. Yu [20] identified three regimes for resonator damping: (1) insufficient damping, (2) excess damping, and (3) optimal damping.

Insufficient damping leads to a very narrow resonance peak in the resonator system. When this resonator is coupled to the enclosure mode, energy is removed only at frequencies very close to resonance. While this may lead to high attenuation at resonance, the new coupled peaks may be unacceptably high for controlling noise that falls even slightly outside this region.

When a resonator contains excessive damping, much of its effect can be nullified. Effective resonators present a relatively low impedance to acoustic waves close to the inlet. However, as resistance increases, the input impedance presented by the resonator approaches the impedance

seen at the enclosure wall. This leads to an ineffective system, in which very little energy is dissipated in the resonator.

By controlling the damping present in the resonator system, it is possible to attenuate the enclosure mode as well as the two coupled resonant peaks. The attenuation observed at resonance will not match that of the first case, but a more broadband effect can be achieved. This optimal damping is often realized by adding a material of low airflow resistance, one layer at a time.

5.1.3 Relative Volume

Lastly, the relative volume between enclosure and resonator cavity also dictates the possible absorption in the coupled system. Fahy [52] derived the coupling between a resonator and enclosure for estimates of possible attenuation. He demonstrated that the separation between the two coupled modes decreases as coupling increases. This coupling is strongly dependent on the ratio of enclosure volume to resonator volume.

While a cavity with a large volume is preferable for energy dissipation, space constraints limit the feasibility of installing bulky resonators. Single Helmholtz resonators with large cavities represent a large centralized footprint that may not fit within available space claims. However, a dual-resonator configuration may provide the same overall volume for effective coupling while allowing space to be distributed more efficiently.

5.2 Experimental Results

In order to validate the theoretical predictions from the previous section, several resonators were designed and coupled to a test enclosure. The enclosure had the same dimensions and geometries as the COMSOL model. Each face was mounted to a steel frame that was designed for structural stability. The front face was made of ⅛ inch clear acrylic. All other faces consisted of ¾ inch

plywood sheets and the bottom sat on a tile floor. The enclosure used for testing is seen in Fig. 5.3.

For surveying the enclosure modes without any resonators present, a loudspeaker was placed in several locations within the enclosure. Figure 5.4 shows the various placements and orientations of the loudspeaker for exciting the enclosure. Microphones were placed very close to walls at approximately ceiling height to avoid measuring near nodal planes. Figure 5.4 also shows the microphone locations in the *x*-*y* plane.

Figure 5.5 shows the measured response of the enclosure without any coupled resonators. The lowest frequency peak (at about 50 Hz) corresponds to the floor-to-ceiling mode of the room in

Figure 5.3 Enclosure used for testing the coupling between various resonator arrays and the enclosure.

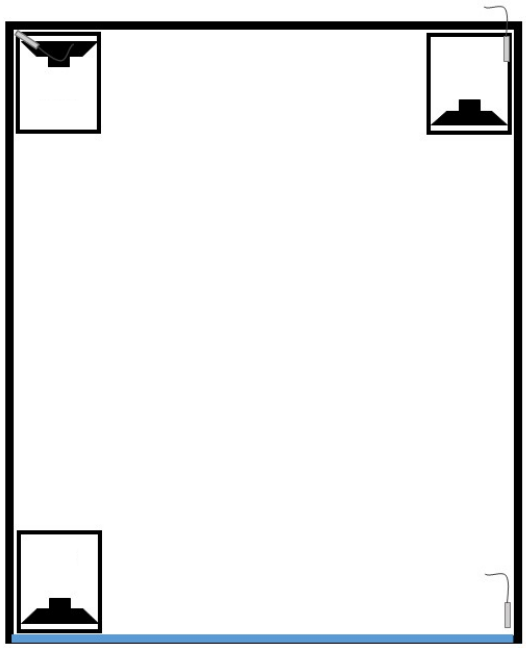

Figure 5.4 Schematic of loudspeaker and microphone placement for survey of enclosure modes.

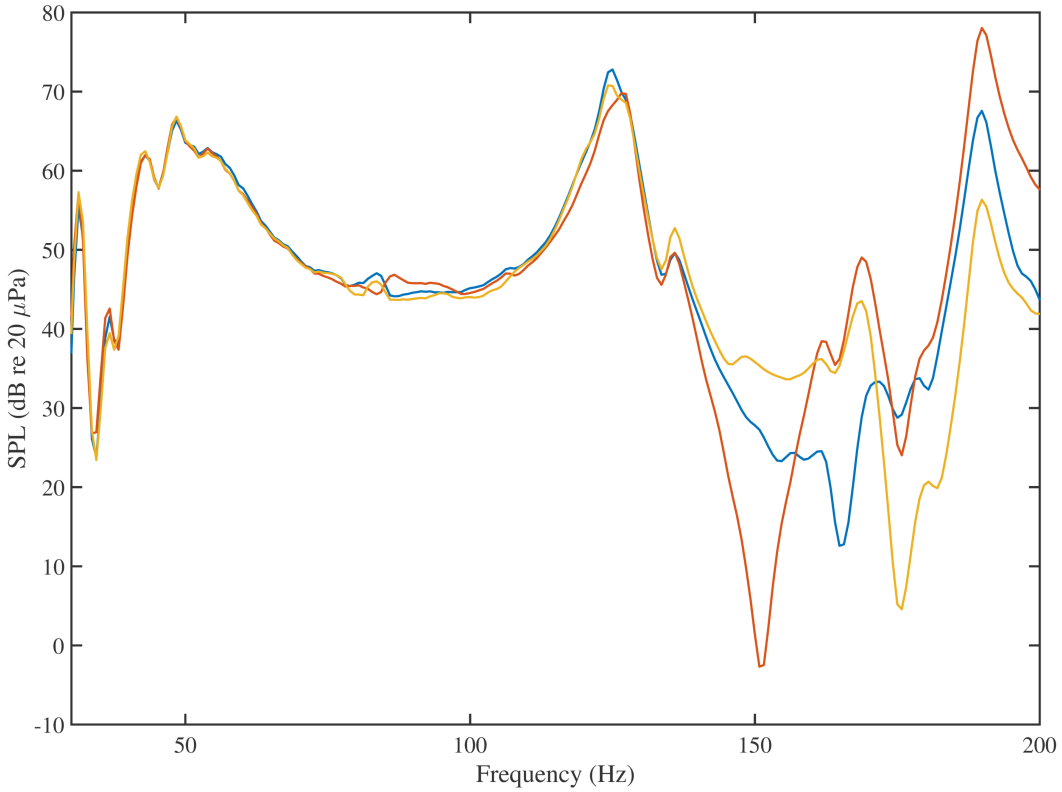

Figure 5.5 Measured response of enclosure before resonator coupling.

which the enclosure was located. For the first enclosure resonance, the COMSOL model and actual results display an interesting discrepancy. The lowest mode for the enclosure was predicted to be 114.92 Hz in COMSOL. However, measured results show a resonance at 125 Hz.

Additional tests were performed with the enclosure away from any exterior walls and with the loudspeaker outside of the enclosure. These tests consistently yielded resonances between 124 Hz and 125 Hz, suggesting that the COMSOL model was inaccurate for the physical properties of the enclosure. Therefore, resonator systems were designed with primary resonances at the measured fundamental mode of the physical enclosure. Furthermore, the dimensions of the COMSOL model were adjusted to yield a resonance in a range similar to the measured enclosure.

Acoustic resonators were modeled using the impedance translation method. Frequency-depen-

dent end corrections from Eqs. (2.5)–(2.7) were applied for all sharp discontinuities within the system. The traditional end correction given in Eq. (2.1) for a baffled resonator was applied at the inlet to the resonator system.

Data were collected using ½ inch electret condenser microphones. One microphone was positioned at the ear location of a typical operator and another was placed very close to the enclosure wall. The loudspeaker was placed in the corner of the enclosure. Sound pressure level (SPL) was recorded at each measurement position using autospectra calculated by the Brüel & Kjær Pulse system. Coherence of each measured signal relative to the reference signal was monitored for each test. Only data that exceeded coherence of 0.95 for the frequency range of interest were considered for this study.

Two ideal-geometry resonators were modeled and constructed at the frequency observed in the uncoupled enclosure as seen in Figs. 5.6–5.7. The single resonator depicted in Fig. 5.6 had a neck with a 2.02 cm radius and a 15.66 cm length. The cavity radius was 4.76 cm and its length was 16.4 cm. The dimensions of the dual-resonator system in Fig. 5.7 are given in Table 5.1. Figure 5.8 shows the enclosure response with and without each of these resonators. The response shows agreement with theoretical predictions for the coupling of undamped resonators to enclosures. Additionally, the dual resonator had a relatively broader absorption bandwidth than the single resonator.

Next, polyester carpet was introduced at the orifice to observe effects of added damping. These results can be seen in Fig. 5.9. Due to the added damping results in Chapter 2, polyester carpet without PET substrate was used to mimic a typical vehicle interior without jeopardizing the performance of the system.

From the results in Figs. 5.8–5.9, it is seen that much of the attenuation is lost with the introduction of polyester carpet. Therefore, practical applications in similar enclosures should refrain from orifice coverings with flow resistivity that exceeds that of polyester carpet.

Figure 5.6 Photo of single Helmholtz resonator coupled to enclosure.

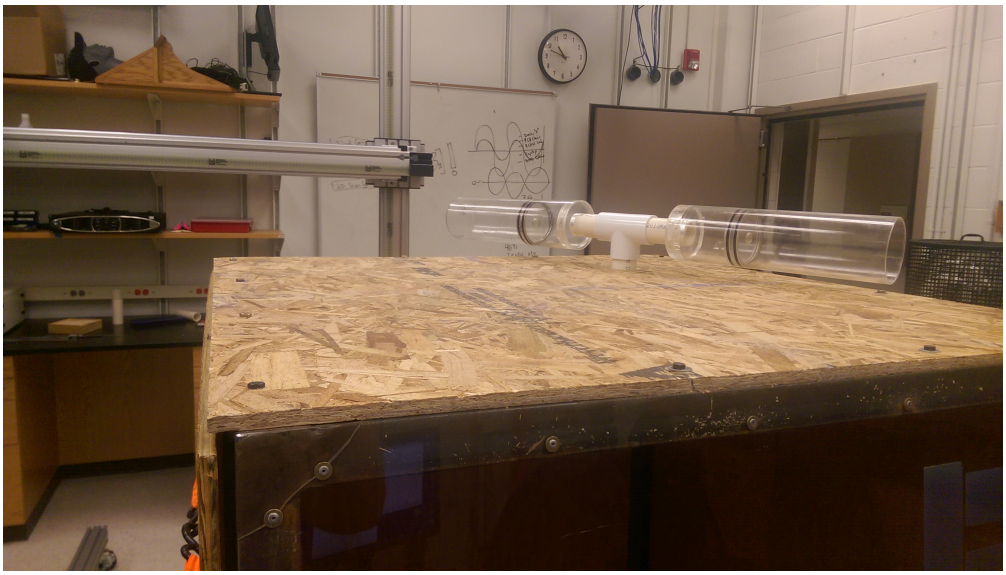

Figure 5.7 Photo of dual Helmholtz resonator system coupled to enclosure.

Table 5.1 Dimensions of dual-resonator system for coupling measurements.

Resonator Dimensions				
	L_V (cm)	r_V (cm)	L_N (cm)	r_N (cm)
Resonator 1	10.45	4.76	7.96	2.03
Resonator 2	10.45	4.74	8.01	2.03

T-Junction Dimensions		
	L_T (cm)	r_T (cm)
Branch 1	1.4	2.42
Branch 2	1.0	2.42
Branch 3	1.2	2.42

Side Branch Dimensions		
	L_S (cm)	r_S (cm)
Side Branch	5.75	2.02

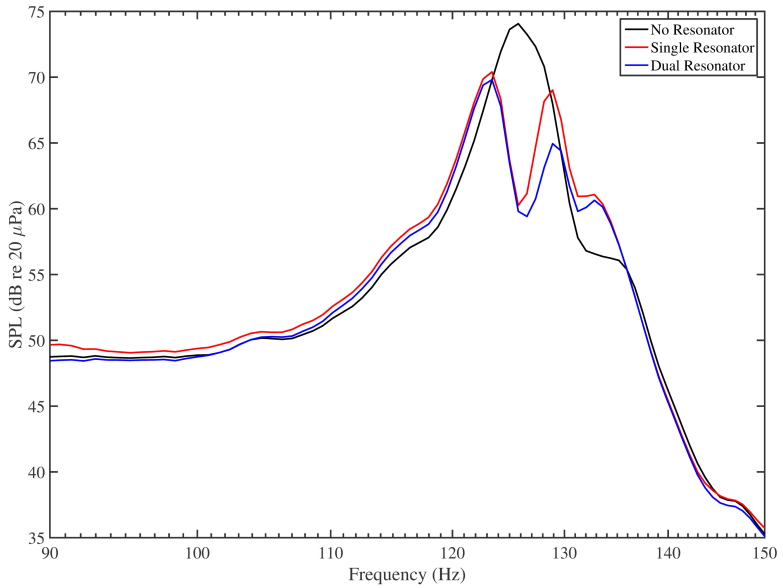

Figure 5.8 Comparison of enclosure response with and without acoustic resonators.

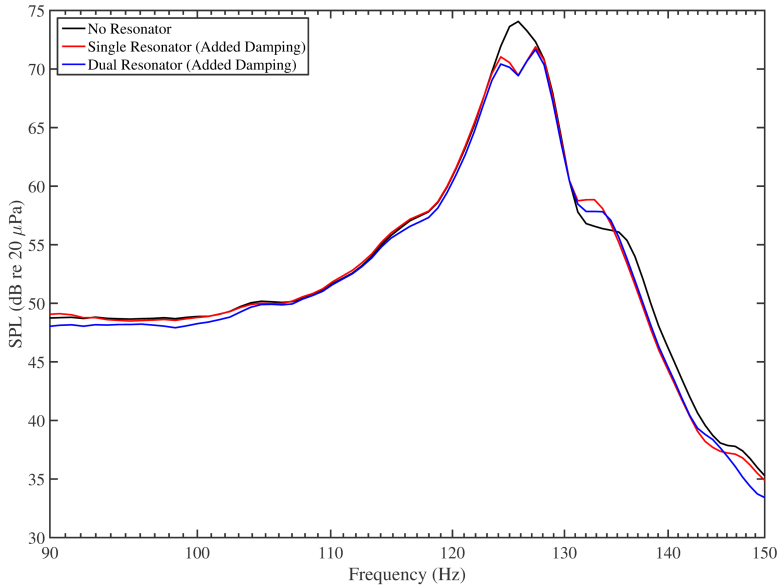

Figure 5.9 Comparison of enclosure response with and without damped acoustic resonators. Polyester carpet was placed at the mouth of each acoustic resonator system.

5.3 3D-Printed Resonator System

Since the dimensions of the resonators tested above were impractical for installation, a compact resonator junction was fabricated using 3D-printing techniques. The component, seen in Fig. 5.10 was designed according to space constraints similar to those found in typical vehicle interiors.

Figure 5.10 Image of 3D-printed component designed for enclosure coupling.

The part was then attached to the adjustable cavities and its input acoustic impedance was tested in an impedance tube as seen in Fig. 5.11. Table 5.2 contains the dimensions of the 3D-printed resonator system. The results of this test are shown in Fig. 5.12. The measured acoustic impedance agrees reasonably well over frequency with the modeled predictions, although there is some discrepancy in magnitude. This is most likely due to the internal roughness present due to the 3D-printing process.

A complete model of the 3D-printed component–including coupled cavities–was built in COMSOL and coupled to the enclosure. The coupled and uncoupled SPL at resonance were found using an eigenfrequency study. Figure 5.13 shows the predicted effect of the 3D-printed resonator system. The results in Fig. 5.13 agree with the theoretical prediction for coupling. The original mode

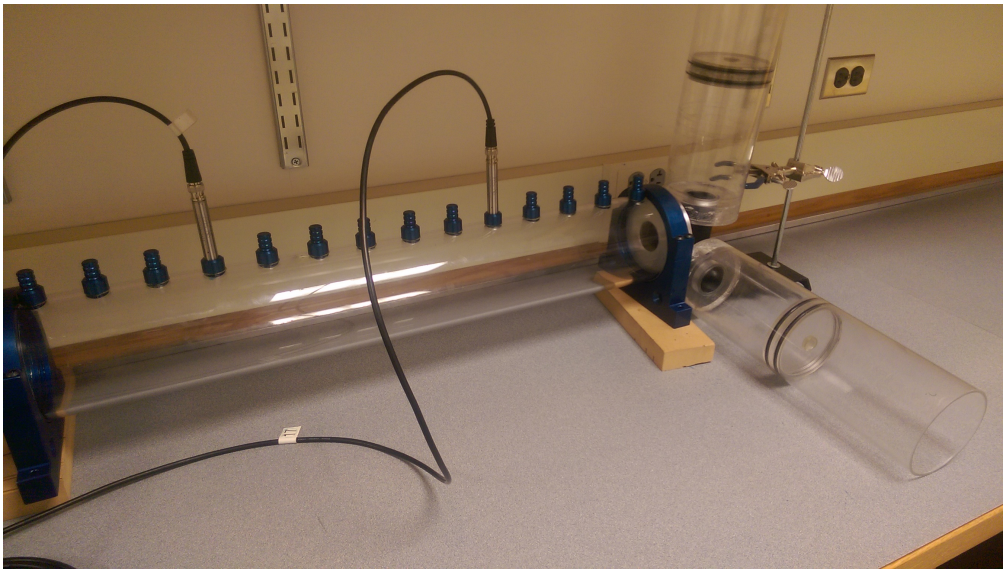

Figure 5.11 Setup of impedance tube measurements of 3D-printed resonator system.

Table 5.2 Dimensions of 3D-printed resonator system for acoustic impedance tests. Resonator 1 consists of a straight neck, while Resonator 2 has an additional curved segment.

Resonator Dimensions						
	L_V (cm)	r_V (cm)	L_N (cm)	Bend angle	L_m (cm)	r_N (cm)
Resonator 1	14.76	4.76	2.9	—	—	2.01
Resonator 2	14.12	4.74	2.7	90°	4.5	2.01

Side Branch Dimensions		
	r_S (cm)	L_S (cm)
Side Branch	2.01	5.4

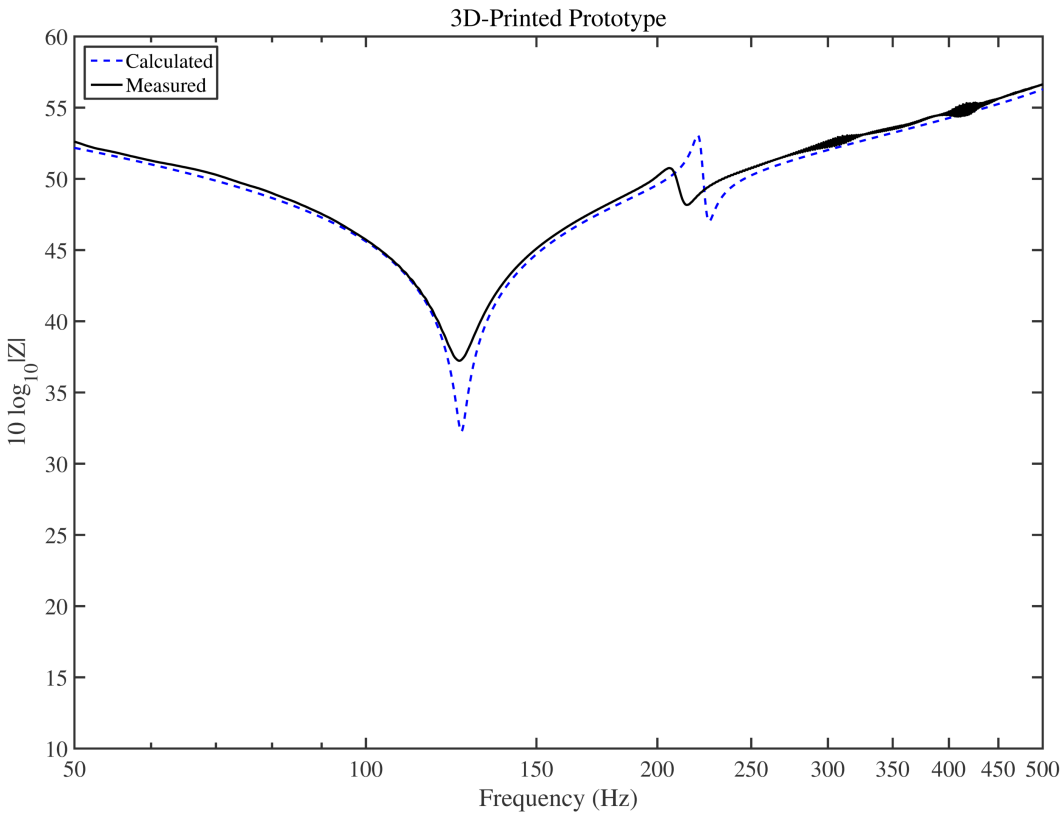

Figure 5.12 Acoustic impedance of 3D-printed resonator system.

at 126.52 Hz is split into two peaks of lower amplitude at 125 Hz and 139.1 Hz.

The 3D-printed prototype was then coupled to the actual enclosure to observe its effect on the target resonance. Figure 5.14 shows enclosure with the prototype attached. The resonator was tested with and without a layer of loudspeaker grill cloth over the inlet. Data were taken at six points within the enclosure, including the nominal position of an operator's ear. As seen in Fig. 5.15, the microphones were distributed throughout the enclosure. Three microphones were placed close to boundaries to avoid nodal planes, while the remaining three were placed away from boundaries. Each of the odd-numbered microphones correspond to a position adjacent to a wall. Microphone 2 lies at the ear level of a typical seated occupant of the space. Microphones 4 and 6 were placed at random locations within the volume of the enclosure. Figure 5.16 shows the

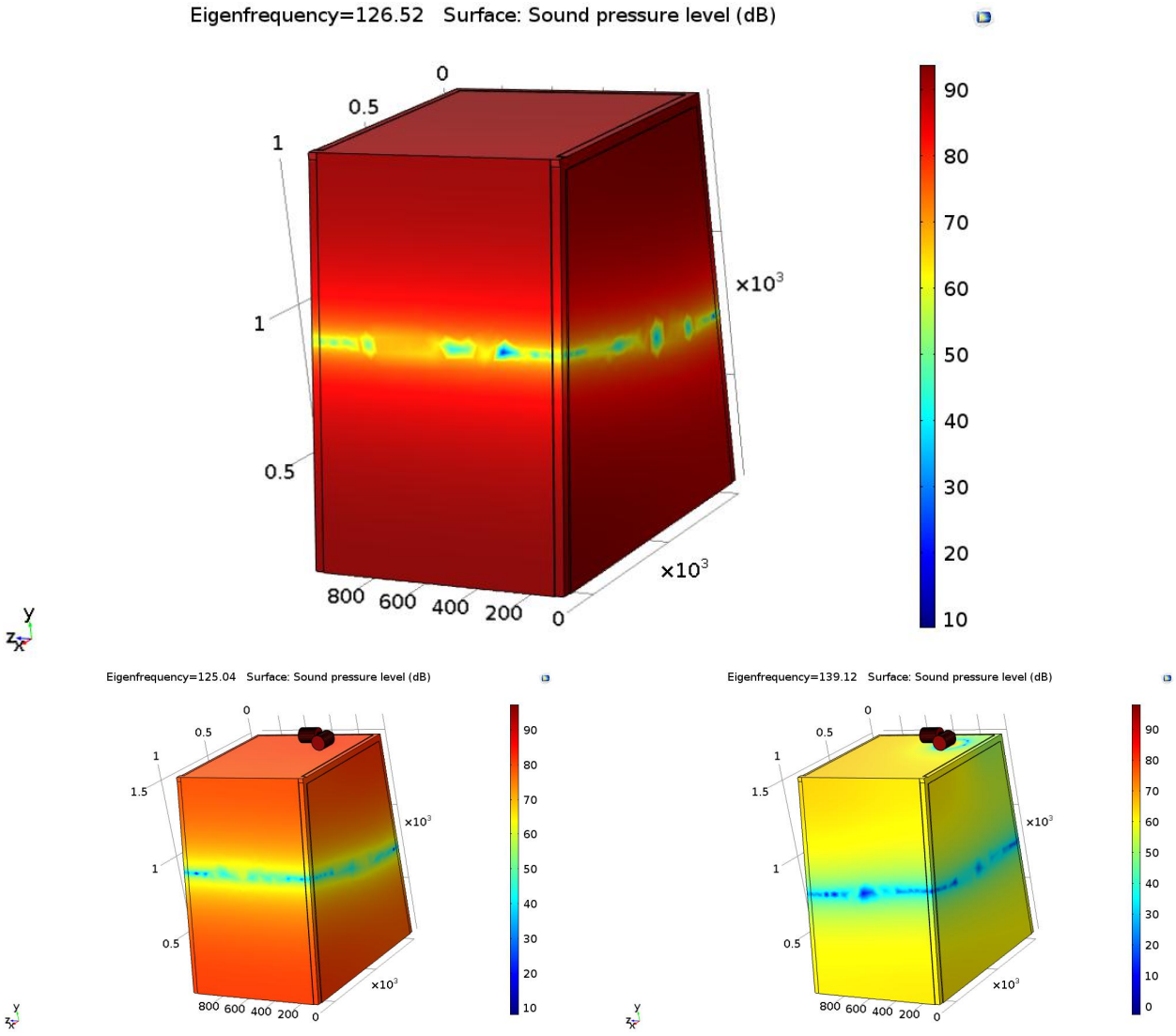

Figure 5.13 Modeled SPL at enclosure resonance with and without coupled resonator system. The upper plot shows the shape and SPL of the lowest enclosure mode. The lower two plots show each of the closely-spaced coupled resonances.

response of the system with each damping condition at the ear location.

The undamped response shows attenuation consistent with the target levels for this study. At resonance, the observed attenuation is about 15 dB. There is at least 10 dB of attenuation over a bandwidth of 10 Hz. Adding one layer of loudspeaker grill cloth decreases the coupling between the two systems and diminishes the effect of the resonator. Adding additional damping further diminished the absorption capabilities of the resonator.

Figure 5.17 shows a comparison of SPL at each of the six microphone positions with and without a coupled resonator. Each microphone shows at least 10 dB of attenuation over the desired frequency bandwidth. The low SPLs at microphones 4 and 6 suggest that both were close to a nodal plane.

The results in Figs. 5.16–5.17 suggest that the undamped 3D-printed resonator system will achieve the design goals for this research. The undamped resonator contains sufficient internal resistance, so added treatment is unnecessary for broadening its response.

Figure 5.14 Photo of 3D-printed resonator system coupled to enclosure.

Figure 5.15 Photo of microphone and loudspeaker positions for testing 3D-printed resonator system.

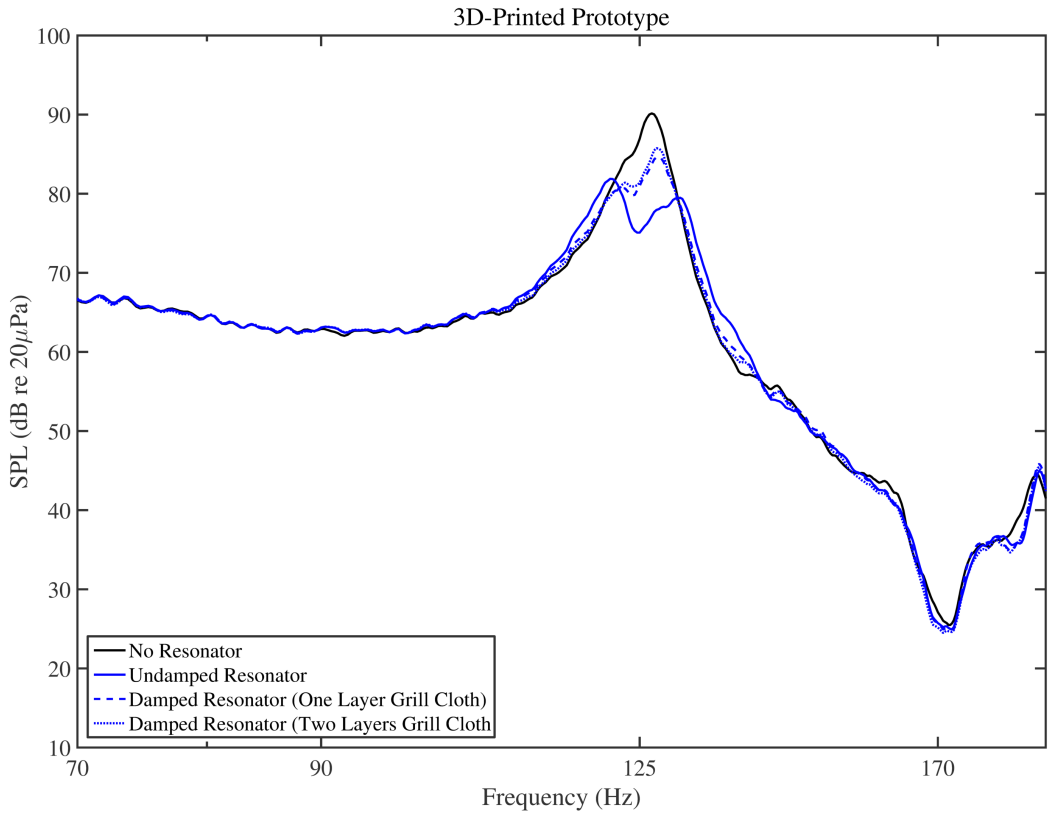

Figure 5.16 SPL at the ear level of an operator with and without the 3D-printed resonator. The coupled response with one and two layers of loudspeaker grill cloth is also shown.

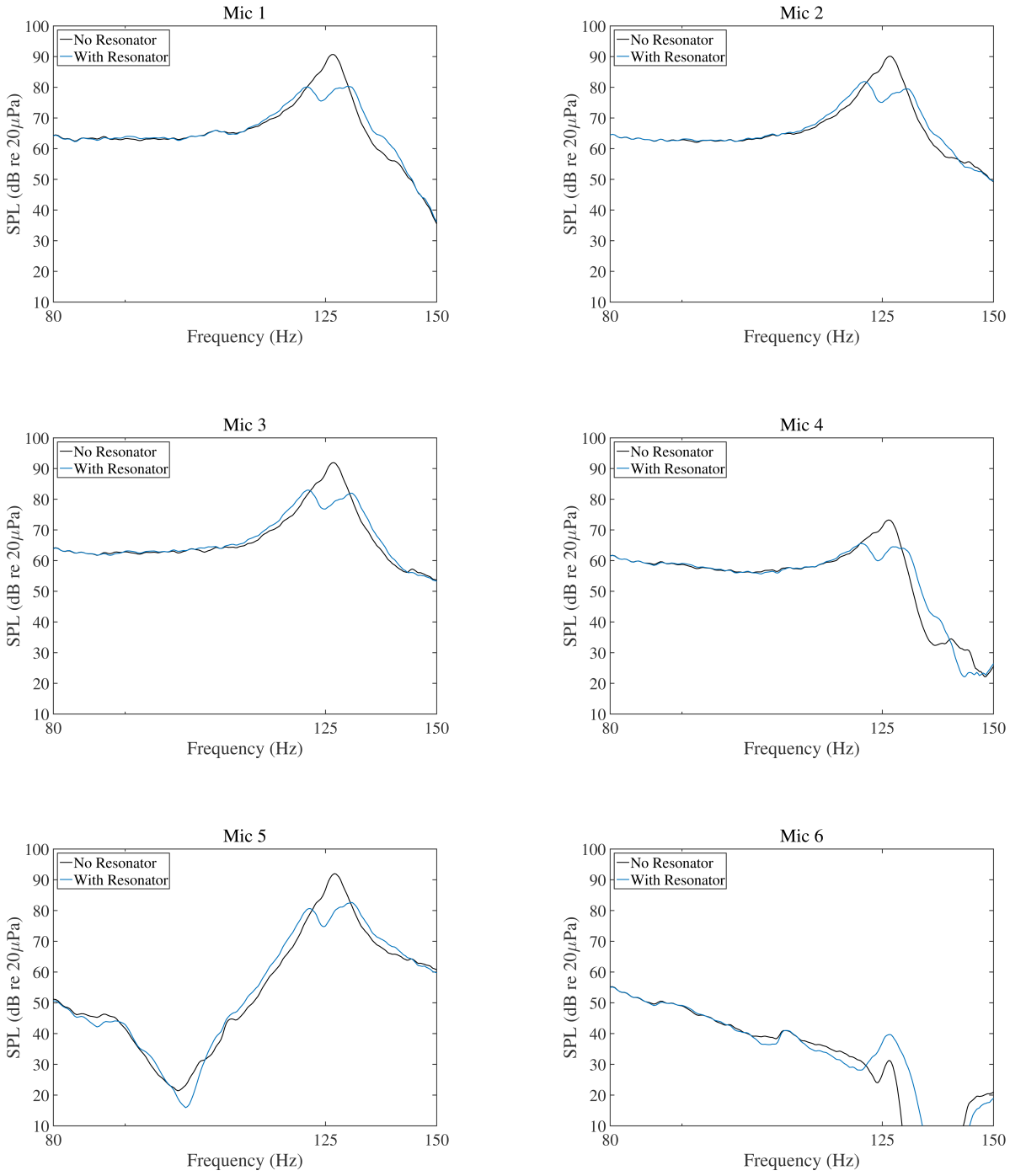

Figure 5.17 Comparison of SPL for the coupled and uncoupled enclosure at six microphone positions

Chapter 6

Conclusions

Noise control presents a number of benefits to both manufacturers and operators. First, it allows many of the physiological and psychological effects associated with noise to be reduced or eliminated. Noise control also offers a competitive advantage to manufacturers. Furthermore, passive attenuation of noise can be achieved using relatively cheap and durable materials. The present research aimed to improve upon classical formulations for ideal-geometry systems of resonators and to develop new, computationally efficient methods for predicting the response of nonideal geometry systems. These resonator systems were then used to attenuate a modal peak in a small enclosure.

6.1 Summary of Methods

General characteristics found in most systems of resonators were explored in detail. Considerations were made for different end corrections as well as thermoviscous losses at tube walls. Airflow resistivity data provided for various materials were incorporated into the model to account for the effect of facing treatments. These resistive elements were applied to resonator arrays and tested in an impedance tube using the two-microphone method.

Classical lumped-element formulations for the acoustic impedance of resonators were compared to the impedance translation formula. The simple lumped element method was modified to preserve higher-order terms and was also compared to the impedance translation theorem. Test resonators with adjustable volume and various neck lengths were constructed to validate the accuracy of each method. The two microphone method was used to extract transmission loss and acoustic impedance data.

Ideal-geometry resonators were combined in a series-parallel configuration and modeled using each of the modeling techniques. Special consideration was given to modeling a practical T-junction. The accuracy of each method was assessed based on acoustic impedance data.

In order to meet space requirements, acoustic resonators containing nonideal geometries were also studied. Helmholtz resonators with tapered necks were modeled using existing theory. The theory was tested against measured acoustic impedance data for a fabricated tapered-neck Helmholtz resonator. The original expressions were modified and compared to the existing theory. Additionally, a novel impedance translation method for considering curved Helmholtz resonators was developed using theory for curved ducts of circular cross section. This theory was compared to the current engineering methods for single resonators and systems of resonators.

Various resonators were coupled to an enclosure to observe attenuation. The enclosure was modeled in COMSOL to predict the general shape of the first few acoustic room modes. The resonator location was selected based on the predicted mode shapes. Sound pressure level was recorded at multiple locations inside the enclosure with and without coupled resonators. Damping was incrementally added to the mouth of the resonators to explore the effect on coupling.

6.2 Summary of Findings

The impedance translation theorem was shown to accurately model arbitrary systems of resonators. The lumped element method and its higher-order approximations exhibited good agreement with measured results for very simple resonators at low frequencies. However, as both system complexity and frequency increased, both the lumped element method and element-by-element method lost considerable accuracy. Impedance translation was shown to preserve wave effects throughout entire distributed systems while the other two methods did not.

The original theory for tapered necks was found to under-predict the resonance of a single, tapered-neck Helmholtz resonator. By adding higher-order approximations to the cavity and improving the end corrections of the original model, theoretical predictions were brought into better correspondence with the measured results. However, a taper was not applied to the current application due to the increased fundamental frequency and only minimal increase on the overall efficiency.

The modified impedance translation theorem for curved Helmholtz resonators accurately predicted the acoustic impedance for toroidal bends. For simple systems with a single curve, the common engineering practice of treating the curve as an equivalent straight length was adequate. However, in systems with multiple bends, the standard method proved to be inaccurate in comparison to that involving the modified impedance translation theorem.

A dual-resonator system with one curved neck was identified as a viable candidate for attenuating noise in the targeted bandwidth of about 15 Hz. This system of resonators achieved 10 dB of attenuation over a bandwidth of 10 Hz at the seated ear position in a simple enclosure.

6.3 Contributions

Accurate, computationally efficient modeling tools were developed for a user to design systems of resonators. They facilitate the prediction of acoustic input impedance for systems of resonators including Helmholtz resonators, T-junctions, tapers, and curved ducts in arbitrary configurations. Added damping can be incorporated when airflow resistivity values are known. A GUI was also developed for rapid acoustic impedance calculations of single ideal-geometry Helmholtz resonators.

The present research builds on the theory for predicting the acoustic impedance of Helmholtz resonators with tapered necks. For the resonators tested in this study, the adjustments greatly improved the accuracy of the calculations.

This research also provides an impedance translation method for modeling the effect of curved necks in Helmholtz resonators. Existing methods for modeling systems with curved Helmholtz resonators do not adequately reflect the behaviors of such systems.

Finally, this study developed a working prototype system of resonators with 10 dB of attenuation over a bandwidth of 10 Hz. This meets the space constraints and attenuation that were targeted for the research.

6.4 Implications and Recommendations

This thesis provides a basis for modeling arbitrary systems of resonators. While tapers of constant slope were analyzed and tested, further research may expand predictions to complex flares. Likewise, the characteristics of toroidal bends with varying radius of curvature may add flexibility to the design of future resonators. While analytical expressions for arbitrary tapers and bends exist, much of the research uses computationally expensive formulations to predict their responses [80, 81]. Much of the existing work on this topic has also been focused on modeling musical instruments [72, 82]. These approaches can be adapted to provide computationally efficient

modeling tools for acoustic resonators.

Internal acoustic resistance may also be explored to understand the contributions of each loss mechanism more fully. Although the overall damping predicted in the model matched measured results, theoretical formulations for radiation resistance in finite baffles and losses at discontinuities should be considered. The model should also be adjusted to account for losses due to surface roughness.

Additional work may be performed to include nonideal geometries other than curves and tapers. Cavities with nonideal geometries should be explored to optimize space usage. While most simple models account only for cavity volume, the effects of different cavity shapes can be explored in greater detail. Although some design guides have been given [41,42], most studies rely heavily on experimental data and boundary element modeling [83, 84]. Practical analytical methods may be developed to predict the response of arbitrary cavity geometries.

The GUI may be modified and extended to allow engineers to graphically design complex systems of resonators. The existing tool allows users to quickly and accurately design individual Helmholtz resonators in a variety of configurations, but it should be expanded to offer the ability to design arbitrary systems of resonators with complex geometries.

Further work should be done to better understand resonator coupling to enclosures. Resonator placement, damping, and relative volume may be optimized to provide the highest attenuation possible. Current research relies heavily on either empirical observations [85] or sophisticated algorithms [20, 54]. Empirical treatments of coupling typically lack accuracy and apply only to the simplest cases. Complicated algorithms are often computationally expensive and require extensive detail to be built into each case. Neither method is well-suited to the rapid prototyping and accuracy required for many engineering applications. A hybrid method may be explored to provide computationally efficient and accurate predictions for enclosure-resonator coupling. Furthermore, the possibility of coupling multiple systems of resonators to one enclosure is worth further study.

Bibliography

[1] S. Kuo, "Active Noise Control: A Tutorial Review," Proceedings of the IEEE **87,** 943–973 (1999).

[2] S. M. Kuo and D. Morgan, *Active noise control systems: algorithms and DSP implementations* (John Wiley and Sons, 1995).

[3] C. D. Kestell and C. H. Hansen, "An overview of active noise control," Safety in Action (1998).

[4] D. R. Morgan, "A hierarchy of performance analysis techniques for adaptive active control of sound and vibration," The Journal of the Acoustical Society of America **89,** 2362–2369 (1991).

[5] C. Zwikker and C. W. Kosten, *Sound absorbing materials* (Elsevier, 1949).

[6] M. Vitruvius Pollio and F. Granger, *On architecture* (Cambridge: Harvard University Press, 1983).

[7] S. Polychronopoulos, D. Kougias, P. Polykarpou, and D. Skarlatos, "The use of resonators in ancient Greek Theatres," Acta Acustica united with Acustica **99,** 64–69 (2013).

[8] J. Landels, "Assisted resonance in ancient theatres," Greece and Rome (Second Series) **14,** 80–94 (1967).

[9] H. L. Helmholtz and A. J. Ellis, *On the Sensations of Tone as a Physiological Basis for the Theory of Music* (Cambridge University Press, 2009).

[10] J. Rayleigh, "On the theory of resonance," Collected scientific papers **1,** 33–75 (1870).

[11] K. Ingard, "On the radiation of sound into a circular tube, with an application to resonators," Journal of the Acoustical Society of America **20,** 665–682 (1948).

[12] K. Ingard, "On the theory and design of acoustic resonators," Journal of the Acoustical Society of America **25,** 1037–1061 (1953).

[13] M. Alster, "Improved calculation of resonant frequencies of Helmholtz resonators," Journal of Sound and Vibration **24,** 63–85 (1972).

[14] P. K. Tang and W. A. Sirignano, "Theory of a generalized Helmholtz resonator," Journal of Sound and Vibration **26,** 247–262 (1973).

[15] A. Selamet, "Circular concentric Helmholtz resonators," Journal of the Acoustical Society of America **101,** 41–51 (1996).

[16] J. Dang, "An experimental study of the open end correction coefficient," Journal of the Acoustical Society of America **104,** 1075–1084 (1998).

[17] V. Pagneux, N. Amir, and J. Kergomard, "A study of wave propagation in varying cross-section waveguides by modal decomposition. Part I. Theory and validation," Journal of the Acoustical Society of America **100,** 2034–2048 (1996).

[18] N. Amir, V. Pagneux, and J. Kergomard, "A study of wave propagation in varying cross-section waveguides by modal decomposition, Part II. Results," Journal of the Acoustical Society of America **101,** 2504–2517 (1997).

[19] Z. L. Ji, "Acoustic length correction of closed cylindrical side-branched tube," Journal of Sound and Vibration **283,** 1180–1186 (2005).

[20] G. Yu, D. Li, and L. Cheng, "Effect of internal resistance of a Helmholtz resonator on acoustic energy reduction in enclosures," Journal of the Acoustical Society of America **124,** 3534–3543 (2008).

[21] M. Terao, "Implementation of a tuning system for Helmholtz resonator arrays in HVAC ducts," Noise Control Engineering Journal **59,** 476–490 (2011).

[22] S. Kim, Y.-H. Kim, and J.-H. Jang, "A theoretical model to predict the low-frequency sound absorption of a Helmholtz resonator array," Journal of the Acoustical Society of America **119,** 1933–1936 (2006).

[23] S.-H. Seo and Y.-H. Kim, "Silencer design by using array resonators for low-frequency band noise reduction," Journal of the Acoustical Society of America **118,** 2332–2338 (2005).

[24] C. Field and F. Fricke, "Theory and applications of quarter-wave resonators: A prelude to their use for attenuating noise entering buildings through ventilation openings," Applied Acoustics **53,** 117–132 (1998).

[25] A. Selamet, N. Dickey, and J. Novak, "The Herschel–Quincke tube: a theoretical, computational, and experimental investigation," Journal of the Acoustical Society of America **96,** 3177–3185 (1994).

[26] G. Stewart, "The theory of the Herschel-Quincke tube," Physical Review **31,** 696–698 (1928).

[27] D.-Y. Maa, "Potential of microperforated panel absorber," Journal of the Acoustical Society of America **104,** 2861–2866 (1998).

[28] L. Huang, "Modal analysis of a drumlike silencer," Journal of the Acoustical Society of America **112,** 2014–2025 (2002).

[29] J. B. Lawrie and I. M. Guled, "On tuning a reactive silencer by varying the position of an internal membranea)," Journal of the Acoustical Society of America **120,** 780–790 (2006).

[30] A. El-Sharkawy and A. H. Nayfeh, "Effect of an expansion chamber on the propagation of sound in circular ducts," Journal of the Acoustical Society of America **63,** 667–674 (1978).

[31] A. Selamet and Z. Ji, "Acoustic attenuation performance of circular expansion chambers with extended inlet/outlet," Journal of Sound and Vibration **223,** 197–212 (1999).

[32] D. D. Davis Jr, G. M. Stokes, D. Moore, and G. L. Stevens Jr, "Theoretical and experimental investigation of mufflers with comments on engine-exhaust muffler design," Technical report (1954) .

[33] M. Munjal, "Recent advances in muffler acoustics," International Journal of Acoustics and Vibration **18,** 71–85 (2013).

[34] M. Long, *Architectural acoustics* (Elsevier, 2005), pp. 836–837.

[35] M. Kleiner and J. Tichy, *Acoustics of small rooms* (CRC Press, 2014), pp. 134–143.

[36] M. Long, *Architectural acoustics* (Elsevier, 2005), p. 769.

[37] F. Karal, "The analogous acoustical impedance for discontinuities and constrictions of circular cross section," Journal of the Acoustical Society of America **25,** 327–334 (1953).

[38] N. Dickey and A. Selamet, "Helmholtz resonators: one-dimensional limit for small cavity length-to-diameter ratios," Journal of Sound and Vibration **195,** 512–517 (1996).

[39] A. Doria, "A simple method for the analysis of deep cavity and long neck acoustic resonators," Journal of Sound and Vibration **232,** 823–833 (2000).

[40] S. K. Tang, C. H. Ng, and E. Y. L. Lam, "Experimental investigation of the sound absorption performance of compartmented Helmholtz resonators," Applied Acoustics **73,** 969–976 (2012).

[41] R. Chanaud, "Effects of geometry on the resonance frequency of Helmholtz resonators," Journal of Sound and Vibration **178,** 337–348 (1994).

[42] R. Chanaud, "Effects of geometry on the resonance frequency of helmholtz resonators, Part II," Journal of Sound and Vibration **204,** 829–834 (1997).

[43] A. Selamet, "Circular asymmetric Helmholtz resonators," Journal of the Acoustical Society of America **107,** 2360–2369 (2000).

[44] S. K. Tang, "On Helmholtz resonators with tapered necks," Journal of Sound and Vibration **279,** 1085–1096 (2005).

[45] W. Rostafinski, "On propagation of long waves in curved ducts," Journal of the Acoustical Society of America **52,** 1411–1420 (1972).

[46] A. Cummings, "Sound transmission in curved duct bends," Journal of Sound and Vibration **35,** 451–477 (1974).

[47] W. Osborne, "Higher mode propagation of sound in short curved bends of rectangular cross-section," Journal of Sound and Vibration **45,** 39–52 (1976).

[48] C. Tam, "A study of sound transmission in curved duct bends by the Galerkin method," Journal of Sound and Vibration **45,** 91–104 (1976).

[49] C. R. Fuller and D. A. Bies, "Propagation of sound in a curved bend containing a curved axial partition," Journal of the Acoustical Society of America **63,** 681–686 (1978).

[50] A. Cabelli, "The acoustic characteristics of duct bends," Journal of Sound and Vibration **68,** 369–388 (1980).

[51] W. Rostafinski, *Monograph on propagation of sound waves in curved ducts* (NASA, 1991).

[52] F. Fahy and C. Schofield, "A note on the interaction between a Helmholtz resonator and acoustic mode of an enclosure," Journal of Sound and Vibration **72,** 365–378 (1980).

[53] A. Cummings, "The effects of a resonator array on the sound field in a cavity," Journal of Sound and Vibration **154,** 25–44 (1992).

[54] P. L. Driesch, "Acoustic control in enclosures using optimally designed Helmholtz resonators," Ph.D. Thesis, The Pennsylvania State University, 2002.

[55] D. Li and L. Cheng, "Acoustically coupled model of an enclosure and a Helmholtz resonator array," Journal of Sound and Vibration **305,** 272–288 (2007).

[56] L. E. Kinsler, A. R. Frey, A. B. Coppens, and J. V. Sanders, *Fundamentals of acoustics* (John Wiley and Sons, 1999), pp. 272–274.

[57] D. A. Bies and C. H. Hansen, *Engineering noise control: theory and practice*, 4 ed. (CRC press, 2009), p. 449.

[58] H. Bass, L. Sutherland, A. Zuckerwar, D. Blackstock, and D. Hester, "Atmospheric absorption of sound: Further developments," Journal of the Acoustical Society of America **97,** 680–683 (1995).

[59] L. E. Kinsler, A. R. Frey, A. B. Coppens, and J. V. Sanders, *Fundamentals of acoustics* (John Wiley and Sons, 1999), pp. 277–280.

[60] P. M. Morse and K. U. Ingard, *Theoretical acoustics* (Princeton university press, 1968).

[61] K. Ingard and R. H. Lyon, "The impedance of a resistance loaded Helmholtz resonator," Journal of the Acoustical Society of America **25,** 854–857 (1953).

[62] T. J. Cox and P. D'Antonio, *Acoustic absorbers and diffusers: theory, design and application* (CRC Press, 2009), pp. 156–160.

[63] I. L. Ver and L. L. Beranek, *Noise and vibration control engineering: principles and applications* (Wiley, 2006), pp. 261–271.

[64] ASTM Standard C522-03, 2009, "Standard Test Method for Airflow Resistance of Acoustical Materials," ASTM International .

[65] T. W. Leishman and B. E. Anderson, "Evaluation of moving-coil loudspeaker and passive radiator parameters using normal-incidence sound transmission measurements: Theoretical developments)," The Journal of the Acoustical Society of America **134,** 223–236 (2013).

[66] W. P. Mason, *Electromechanical transducers and wave filters* (Van Nostrand, New York, 1948), pp. 204–205.

[67] A. D. Pierce *et al.*, *Acoustics: An introduction to its physical principles and applications* (McGraw-Hill, New York, 1981), Vol. 20, pp. 324–330.

[68] J. Chung and D. Blaser, "Transfer function method of measuring in-duct acousics properties I. Theory," Journal of the Acoustical Society of America **68,** 907–913 (1980).

[69] J. Chung and D. Blaser, "Transfer function method of measuring in-duct acousics properties II. Experiment," Journal of the Acoustical Society of America **68,** 914–921 (1980).

[70] H. Boden and M. Abom, "Influence of errors on the two-microphone method for measuring acoustic properties in ducts," The Journal of the Acoustical Society of America **79,** 541–549 (1986).

[71] G. R. Plitnik and W. J. Strong, "Numerical method for calculating input impedances of the oboe," Journal of the Acoustical Society of America **65,** 816–825 (1979).

[72] A. C. P. Braden, "Bore optimisation and impedance modelling of brass musical instruments," Ph.D. Thesis, University of Edinburgh, 2007.

[73] A. G. Webster, "Acoustical impedance and the theory of horns and of the phonograph," Proceedings of the National Academy of Sciences **5,** 275–282 (1919).

[74] V. L. Streeter, E. B. Wylie, and K. W. Bedford, *Fluid Mechanics* (McGraw-Hill, 1998).

[75] W. Rostafinski, "Acoustic systems containing curved duct sections," Journal of the Acoustical Society of America **60,** 23–28 (1976).

[76] W. Rostafinski, "Analysis of propogation of waves of acoustic frequencies in curved ducts," Journal of the Acoustical Society of America **56,** 11–15 (1974).

[77] S. Ko and L. Ho, "Sound attenuation in acoustically lined curved ducts in the absence of fluid flow," Journal of Sound and Vibration **53,** 189–201 (1977).

[78] S. Felix and V. Pagneux, "Sound propagation in rigid bends: A multimodal approach," Journal of the Acoustical Society of America **110,** 1329–1377 (2001).

[79] D. H. Keefe and A. H. Benade, "Wave propagation in strongly curved ducts," Journal of the Acoustical Society of America **74,** 330–332 (1983).

[80] S. Felix and V. Pagneux, "Multimodal analysis of acoustic propagation in three-dimensional bends," Wave Motion **36,** 157–168 (2002).

[81] B. Kolbrek, "Modal sound propagation in curved horns of rectangular cross-section," Ph.D. Thesis, Norwegian University of Science and Technology, 2013.

[82] C. J. Nederveen, "Influence of a toroidal bend on wind instrument tuning," Journal of the Acoustical Society of America **104,** 1616–1626 (1998).

[83] D. A. Hamilton, "Development of a compact intake silencer for a lift truck application," In *Noise-Con Congress and Conference Proceedings*, **248,** 469–477 (2014).

[84] T. Wu, P. Zhang, and C. Cheng, "Boundary element analysis of mufflers with an improved method for deriving the four-pole parameters," Journal of Sound and Vibration **217,** 767–779 (1998).

[85] S. Biswas and A. Agrawal, "Noise reduction in large enclosure using single, dual and ensconced Helmholtz resonators," Current Science **124,** 1681–1691 (2013).